Augmented Ehrenfest dynamics yields a rate for surface hopping

Joseph E. Subotnik[a)]
Department of Chemistry, Northwestern University, 2145 Sheridan Road, Evanston, Illinois, 60208, USA

(Received 17 November 2009; accepted 20 January 2010; published online 7 April 2010)

We present a new algorithm for mixed quantum-classical dynamics that helps bridge the gap between mean-field (Ehrenfest) and surface-hopping dynamics by defining a natural rate of decoherence. In order to derive this decoherence result, we have expanded the number of independent variables in the usual Ehrenfest routine so that mixed quantum-classical derivatives are now propagated in time alongside the usual Ehrenfest variables. Having done so, we compute a unique rate of decoherence using two independent approaches: (i) by comparing the equations of motion for the joint nuclear-electronic probability density in phase space according to Ehrenfest dynamics versus partial Wigner transform dynamics and (ii) by introducing a frozen Gaussian interpretation of Ehrenfest dynamics which allows nuclear wave packets to separate. The first consequence of this work is a means to rigorously check the accuracy of standard Ehrenfest dynamics. Second, this paper suggests a nonadiabatic dynamics algorithm, whereby the nuclei are propagated on the mean-field (Ehrenfest) potential energy surface and undergo stochastic decoherence events. Our work resembles the surface-hopping algorithm of Schwartz and co-workers [J. Chem. Phys. **123**, 234106 (2005)]—only now without any adjustable parameters. For the case of two electronic states, we present numerical results on the so-called "Tully problems" and emphasize that future numerical benchmarking is still needed. Future work will also treat the problem of three or more electronic states. © *2010 American Institute of Physics*. [doi:10.1063/1.3314248]

I. INTRODUCTION: NONADIABATIC DYNAMICS BEYOND THE BORN–OPPENHEIMER APPROXIMATION

The Born–Oppenheimer approximation separates the motion of heavy nuclei from the motion of light electrons, and for many chemical properties and reactions, this separation is reasonable and reliable. Nevertheless, as has been repeatedly emphasized in literature,[1] there are physical situations where the Born–Oppenheimer approximation is not valid and an understanding of nonadiabatic effects is crucial. In particular, in order to correctly describe electron transfer, energy transfer, or any form of electronic relaxation, one must be able to model nonadiabatic effects, where electronic state transitions are exchanged for nuclear kinetic energy (and vice versa).

Currently, several computational algorithms exist for modeling nonadiabatic effects. The computationally cheapest algorithms are local algorithms: one treats the nuclei as classical particles and then propagates a few variables (nuclear and electronic) to simulate the dynamical trajectory of a single system with both nuclear and electronic components. Later, one averages over many mixed quantum-classical trajectories to obtain reliable statistics. Examples of such local models are mean-field Ehrenfest dynamics,[2,3] surface hopping,[4–14] and the Miller–Meyer–Stock–Thoss formalism (MMST),[3,15–17] all of which are discussed below. As far as the current implementations are concerned, Ehrenfest is computationally the cheapest, then surface hopping, and then MMST.

Beyond local methods for nonadiabatic dynamics with a classical flavor, there are, of course, nonlocal methods for nonadiabatic quantum dynamics. In contrast to local methods, nonlocal methods explicitly consider the shapes of nuclear wave packets on several surfaces, an asset that yields additional accuracy—albeit for a higher computational price. By definition, the most expensive such algorithm is full wave packet propagation, which is exact up to the spatial and energy limits specified by the grid size. Less demanding than full wave packet propagation is the *ab initio* multiple spawning technique pioneered by Martinez and co-workers[18,19] and the partial Wigner transform approach studied by Kapral[20,21] and others.[22–30] For partial Wigner transform dynamics, one propagates a joint nuclear-electronic probability density in a classical phase space with a truncated equation of motion.

In this paper, our central purpose is to bridge the gap between Ehrenfest dynamics and partial Wigner transform dynamics and, in so doing, develop a decoherence rate for Ehrenfest dynamics. In order to accomplish this goal, we have augmented standard Ehrenfest dynamics by adding new variables that contain information about nuclear-electronic correlations. These new variables allow us to work with the equation of motion for the Ehrenfest probability in joint nuclear-electronic phase space and thus to compare Ehrenfest dynamics with partial Wigner transform dynamics. Three consequences emerge from our study. First, we develop a means to rigorously check the accuracy of standard Ehrenfest dynamics vis-à-vis partial Wigner transform dynamics. Sec-

[a)]Electronic mail: subotnik@sas.upenn.edu. Present address: Department of Chemistry, University of Pennsylvania.

ond, we show that there is a natural time scale $(1/\tau)$ over which Ehrenfest dynamics fails. Third, using a frozen Gaussian framework, this time scale may be rigorously and independently interpreted as a decoherence time, and we give preliminary evidence that mean-field dynamics with stochastic decoherence events[13,14] introduced at this rate is a powerful new approach to nonadiabatic dynamics.

The outline of this paper is as follows. In Sec. II, we briefly review mixed quantum-classical algorithms currently used to propagate nonadiabatic dynamics. In Sec. III, we formalize Ehrenfest dynamics in joint electronic-nuclear phase space, which requires introducing new dynamical variables [Eqs. (40) and (41)]. In Sec. IV, by comparing it to partial Wigner transform dynamics, we derive a decoherence rate for Ehrenfest dynamics [Eq. (52)] and give a frozen Gaussian interpretation. In Sec. V, we put everything together and give a step-by-step outline of our newly proposed nonadiabatic semiclassical algorithm. In Sec. VI, we give numerical data for our algorithm applied to the three Tully model problems.[5] In Sec. VII, we summarize our results, discuss the strengths and weaknesses of our approach, and suggest future research. For the expert reader who needs no introduction, Eqs. (40), (41), and (52) represent our new contributions to the field of nonadiabatic dynamics.

II. BRIEF REVIEW OF TRADITIONAL NONADIABATIC ALGORITHMS

A. Notational definitions

Before discussing nonadiabatic algorithms, we first establish the necessary notation. We begin with a Hamiltonian having nuclear (R) and electronic (r) degrees of freedom

$$H(r,R) = H^{\mathrm{el}}(r;R) + T_{\mathrm{nuc}}(R). \tag{1}$$

Henceforward, for simplicity of notation, we will focus on the case of only one nuclear degree of freedom almost everywhere (except in Appendix B, where we provide some mathematical details in full generality). All indices for electronic degrees of freedom will be subscript and in Roman characters; when we include them, the distinct nuclear degrees of freedom will always be written in superscript and in Greek characters. Electronic matrices will be written in bold style. We denote m as the mass of an electron and M as the mass of the (single) nucleus.

The standard and direct approach to nonadiabatic quantum dynamics is to expand the complete (nuclear and electronic) wave function in an adiabatic electronic basis $\Phi_i(r;R)$ with nuclear functions $\Omega_i(R,t)$,

$$|\Psi(r,R,t)\rangle = \sum_i \Phi_i(r;R)\Omega_i(R,t). \tag{2}$$

The adiabatic states for the electronic degrees of freedom are defined by

$$H^{\mathrm{el}}(r;R)\Phi_i(r;R) = E_i(R)\Phi_i(r;R). \tag{3}$$

In this basis, the time-dependent Schrödinger equation $i\hbar(\partial\Psi/\partial t)=H\Psi$ becomes

$$i\hbar\frac{\partial}{\partial t}\Omega_j(R,t) = \left(H^{\mathrm{el}}_{jj}(R) - \frac{1}{2M}\frac{\partial^2}{\partial R^2}\right)\Omega_j(R,t) - \frac{1}{2M}\sum_k\left(2d_{jk}(R)\frac{\partial}{\partial R} + g_{jk}(R)\right)\Omega_k(R,t), \tag{4}$$

where the derivative couplings are defined as

$$d_{jk}(R) \equiv \left\langle \Phi_j(r;R)\left|\frac{\partial}{\partial R}\Phi_k(r;R)\right.\right\rangle, \tag{5}$$

$$g_{jk}(R) \equiv \left\langle \Phi_j(r;R)\left|\frac{\partial^2}{\partial R^2}\Phi_k(r;R)\right.\right\rangle. \tag{6}$$

As written, Eq. (4) requires propagating wave packet dynamics over multiple surfaces, which is not feasible in more than a few dimensions. The goal of semiclassical nonadiabatic dynamics is to solve Eq. (4) approximately using a modified version of classical dynamics.

B. Ehrenfest dynamics

The simplest algorithm for semiclassical nonadiabatic dynamics is the mean-field (Ehrenfest) model,[2,3] where, at any nuclear configuration, we guess that the electronic wave function Ψ is a linear combination of adiabatic states $\{\Phi_i\}$ whose coefficients do not depend on the nuclear coordinate,

$$\Psi(r;R(t)) = \sum_i c_i(t)\Phi_i(r;R(t)). \tag{7}$$

Applying the time-dependent Schrödinger equation, $i\hbar(\partial\Psi/\partial t)=H\Psi$, to Eq. (7), we find that along the nuclear trajectory $R(t)$,

$$\frac{dc_j}{dt} = -\frac{i}{\hbar}\sum_k H^{\mathrm{el}}_{jk}(R(t))c_k(t) - \frac{P}{M}\sum_k d_{jk}(R(t))c_k(t). \tag{8}$$

For the density matrix, $\sigma_{ij}=c_j^*c_i$, the equation of motion is

$$\frac{d\sigma_{ij}}{dt} = -\frac{i}{\hbar}\sum_k (H^{\mathrm{el}}_{ik}\sigma_{kj} - \sigma_{ik}H^{\mathrm{el}}_{kj}) - \frac{P}{M}\sum_k (d_{ik}\sigma_{kj} - \sigma_{ik}d_{kj}). \tag{9}$$

Finally, according to Ehrenfest dynamics, the nuclei are propagated on the mean-field potential energy surface

$$\dot{R} = \frac{P}{M}, \tag{10}$$

$$\dot{P} = -\sum_{kl}\sigma_{kl}F_{lk}, \tag{11}$$

where we have defined the (negative) "force"

$$F_{jk}(R) = \langle\Phi_j(r;R)\left|\frac{\partial H^{\mathrm{el}}(r;R)}{\partial R}\right|\Phi_k(r;R)\rangle. \tag{12}$$

While Eq. (10) is merely the definition of momentum, Eq. (11) reflects the mean-field nature of Ehrenfest dynamics. Namely, the nuclei move on the mean-field potential en-

ergy surface rather than multiple nuclear wave packets moving on multiple surfaces. The subsequent shortcomings of Ehrenfest dynamics are well known. For instance, Ehrenfest dynamics cannot well describe bond making or bond breaking, where the nuclear wave packet must begin and end on a single adiabatic surface rather than on a mean-field surface. After all, the average motion of (i) a covalent bond and (ii) a broken bond is not very meaningful: either the two fragments are attached or they are not. In general, one fatal flaw of Ehrenfest dynamics is its inability to capture the effect of multiple nuclear wave packets moving along and separating on different surfaces (which is a form of decoherence).

C. Surface-hopping dynamics

For dynamics calculations, the usual correction for, or alternative to, Ehrenfest dynamics is to apply a surface-hopping algorithm, whereby the nuclei move along one potential energy surface and stochastically hop to other surfaces, with a rate determined by some predetermined criterion.

Many different flavors of surface hopping exist. Thus far, the most commonly used brand is fewest switches surface hopping (FSSH) suggested by Tully in 1990.[5,6] In this approach, one chooses the minimal hopping rate between states so that, for a swarm of particles, the fraction of particles moving along surface k matches the instantaneous electronic population σ_{kk}, the latter being propagated independently. Other versions of surface hopping have been proposed by Rossky,[8,10,11] Prezhdo,[9] and Schwartz,[13,14] each with different surface-hopping criteria. As shown by Truhlar and co-workers,[31–36] surface-hopping algorithms can also be combined with Ehrenfest dynamics for additional accuracy. For a brief recent review of the relevant techniques, see Ref. 13 and 14. To date, most surface-hopping algorithms in the literature can be justified only empirically, by comparison with exact results. The great successes of surface hopping are (i) the ability to treat bond making and breaking and (ii) the ability to close all energetically inaccessible channels during scattering events.

Among the different surface-hopping models listed above, the mean field with stochastic decoherence (MF-SD) algorithm of Larsen, Bedard-Hearn, and Schwartz[13,14] has been a particular inspiration for our research below. In 2005, by using a frozen Gaussian approximation, Schwartz and co-authors derived a rate (γ_k) for the decoherence of the nuclear wave packet on surface k from the mean-field wave packet

$$\gamma_k = \frac{\sigma_{kk}}{\tau_k} dt, \tag{13}$$

$$\frac{1}{\tau_k} = \frac{|\Sigma_{ij} F_{ij} \sigma_{ji} - F_{kk}| a_n}{\hbar}, \tag{14}$$

where dt is the time step of the algorithm, γ_k is the probability of decoherence during any time step, τ_k^{-1} is the rate of decoherence per unit of population in state k, and a_n is the width of the "Ehrenfest wave packet." Schwartz and co-workers then suggested doing Ehrenfest dynamics with stochastic decoherence events at the rate of Eq. (13), and they demonstrated that for the Tully model problems, doing so yielded a correction to standard Ehrenfest dynamics. In this way, they also avoided propagating an independent electronic density matrix which did not correspond to the instantaneous potential energy surface.

Unfortunately, while the MF-SD algorithm has many attractive features, Eqs. (13) and (14) have the essential drawback of requiring the width of a nuclear wave packet in order to apply the frozen Gaussian approach. Although Schwartz and co-workers found that the instantaneous de Broglie wavelength was a reasonable guess

$$a_n = \lambda_D(t) \equiv \frac{\hbar}{mv}, \tag{15}$$

$$\frac{1}{\tau_k} = \frac{|\Sigma_{ij} F_{ij} \sigma_{ji} - F_{kk}|}{|P|}, \tag{16}$$

they also found that this ansatz needed a correction when applied to the one-dimensional Tully problems. For one-dimensional problems, they suggested scaling the thermal wavelength by w, where w is a dimensionless parameter, defined as the "width" of the nonadiabatic coupling element in suitably chosen units. In general, this estimate is unsatisfying because choosing w for multidimensional problems may not be possible (and the suitable units may be unclear). Moreover, the goal of all semiclassical nonadiabatic algorithms is to model nonadiabatic transitions using only local information about the potential energy surface.

Notwithstanding these deficiencies, the Schwartz algorithm has been a key inspiration for the present work, as will become clear. In fact, this research project began with our attempt to find an approximate width a_n to plug into Eq. (14). Although our final nonadiabatic algorithm does not include Eq. (14), our final result [Eq. (52) in Sec. IV) can be interpreted using a frozen Gaussian framework and has clear similarities to Eq. (14).

D. MMST

Although we will not pursue the MMST approach in this paper, we mention that there is a semiclassical approach to nonadiabatic dynamics that avoids surface hopping entirely and can be rigorously justified. The MMST algorithm treats electronic and nuclear motion equivalently by introducing an action angle variable to represent an electronic degree of freedom. Combined with a method to do semiclassical nuclear dynamics for an initial value representation, the MMST approach correctly describes the most difficult nonadiabatic effects including nuclear decoherence. Interestingly, Ehrenfest trajectories appear naturally within the MMST formalism. In the future, it may be fruitful to analyze the decoherence rate presented below in the context of the MMST approach.

E. Partial Wigner transform dynamics

While Ehrenfest dynamics is the quickest and dirtiest way to do nonadiabatic dynamics, a much more rigorous semiclassical approach to understanding mixed quantum-classical dynamics is to represent the nuclear and electronic

system by a partial Wigner transform. Let the total wave function be denoted $|\Psi(t)\rangle$. As shown by Kapral[20,21] and others,[22–30] a natural representation of $|\Psi(t)\rangle$ is a partial Wigner transform over only the classical degrees of freedom. Using the notation from Sec. II A, we define

$$A_{ij}^{W}(R,P,t) \equiv \frac{1}{2\pi\hbar}\int dX e^{iPX/\hbar}\langle \Phi_i;R-X/2|\Psi(t)\rangle \times\langle \Psi(t)|\Phi_j;R+X/2\rangle, \quad (17)$$

where X is an arbitrary point in nuclear coordinate space that serves as a dummy variable. As we evolve in time, the equation of motion for the partial Wigner transform is [to first order in $(m/M)^{1/2}$],[20]

$$\frac{\partial}{\partial t}A_{ij}^{W}(R,P,t) = \frac{-i}{\hbar}\left(\sum_k H_{ik}^{\mathrm{el}}(R)A_{kj}^{W}-A_{ik}^{W}H_{kj}^{\mathrm{el}}(R)\right) - \frac{P}{M}\sum_k \left(d_{ik}(R)A_{kj}^{W}-A_{ik}^{W}d_{kj}(R)\right)-\frac{P}{M}\frac{\partial A_{ij}^{W}}{\partial R} + \frac{1}{2}\sum_k\left(F_{ik}(R)\frac{\partial A_{kj}^{W}}{\partial P}+\frac{\partial A_{ik}^{W}}{\partial P}F_{kj}(R)\right). \quad (18)$$

Equation (18) is a rigorous semiclassical approach to nonadiabatic dynamics that correctly captures the dynamics of nuclei moving on different potential energy surfaces. For this reason, many research groups have investigated how to solve this equation. Intriguingly, Kapral and co-workers[20,21] noted that such equations can be solved by integrating over trajectories with a certain kind of surface hops and "momentum jumps." For our part, we have found that understanding and manipulating the differences between Eqs. (18) and (30) (below) can be very useful.

III. THEORY: EHRENFEST DYNAMICS IN PHASE SPACE

A. Equation of motion for the mean-field joint nuclear-electronic probability density

Equations (9)–(11) completely describe Ehrenfest dynamics, whereby the electronic state of the system and the classical coordinates of the nuclei are propagated together in one trajectory. These equations are local in the sense that the nuclei are treated classically (i.e., as point particles) and there is no nuclear wave packet of any width. Beyond these local equations, however, our immediate goal is to construct an equation of motion for the global joint nuclear-electronic probability density corresponding to a swarm of classical particles in phase space undergoing Ehrenfest dynamics. Just as Langevin dynamics yields a probability density that satisfies the Fokker–Planck equation, we seek an equation of motion for the joint nuclear-electronic probability density for a swarm of particles undergoing Ehrenfest dynamics. Our long term goal is to connect Ehrenfest dynamics with partial Wigner transform dynamics in phase space [i.e., Eq. (18)] (see Table I).

With these goals in mind, suppose that at time $t=0$, our mixed quantum-classical system can be initially represented by a swarm of classical particles distributed in phase space

TABLE I. One new result in this paper is Eq. (30), which is an equation of motion for the joint electronic-nuclear probability density over all phase space when individual particles are moving according to Ehrenfest dynamics (under the unique preimage assumption). There is a natural correspondence between this equation and the Fokker–Planck equation. Ideally, nonadiabatic quantum dynamics would be most easily described by propagating local coordinates corresponding to partial Wigner transform dynamics: this can also be done, albeit within certain approximations (e.g., see Refs. 20, 21, and 37 and citations therein).

	Nuclear only	Joint nuclear-electronic	Joint nuclear-electronic
Probability Density	Fokker–Planck $f(R,P,t)$	Ehrenfest $A_{ij}^{\mathrm{MF}}(R,P,t)$ [Eq. (30)]	Partial Wigner $A_{ij}^{W}(R,P,t)$ [Eq. (18)]
Local Coordinates	Langevin $R(t),P(t)$	Ehrenfest $\sigma(t),R(t),P(t)$ [Eqs. (9)–(11)]	"Partial Wigner Surface Hopping"

with probability $f(R_0,P_0)$. For simplicity, we assume that the initial electronic state (denoted by $\boldsymbol{\sigma}_0$) is constant among all different starting points for the nuclei. The joint nuclear-electronic probability density distribution for mean-field dynamics is then defined as

$$A_{ij}^{\mathrm{MF}}(R,P,t) \equiv \int dR_0\int dP_0 f(R_0,P_0)\,\delta(R(t;R_0,P_0,\boldsymbol{\sigma}_0)-R) \times\delta(P(t;R_0,P_0,\boldsymbol{\sigma}_0)-P)\sigma_{ij}(t;R_0,P_0,\boldsymbol{\sigma}_0). \quad (19)$$

Note that $\Sigma_i\int dR\int dP A_{ii}(R,P,t)=1$ and A_{ij}^{MF} has units of 1/action. Also, $A_{ij}^{\mathrm{MF}}(R,P,0)=f(R,P)\sigma_{ij}(0)$.

The meaning of Eq. (19) is as follows: given the initial distribution at time $t=0$ in phase space, $f(R_0,P_0)$, and the initial electronic state, $\boldsymbol{\sigma}_0$, we run individual Ehrenfest trajectories on all points for which $f(R_0,P_0)>0$. At time t, we pause and search for all trajectories that have evolved to the classical coordinates (R,P). Although multiple trajectories may have evolved in such a way, consider first the case when only one trajectory reaches (R,P). Denote the original position of the particle at $t=0$ by $(\tilde{R}_0,\tilde{P}_0)$ and the electronic density matrix at time t by $\tilde{\boldsymbol{\sigma}}(t)$. In this case, if we change the coordinates inside the arguments of the delta functions in Eq. (19), we find

$$A_{ij}^{\mathrm{MF}}(R,P,t) = \frac{f(\tilde{R}_0,\tilde{P}_0)\tilde{\boldsymbol{\sigma}}(t)}{|\det(\mathbf{W}(\tilde{R}_0,\tilde{P}_0,t))|}, \qquad \mathbf{W}(t)=\begin{pmatrix}\frac{\partial R(t)}{\partial R_0} & \frac{\partial R(t)}{\partial P_0}\\ \frac{\partial P(t)}{\partial R_0} & \frac{\partial P(t)}{\partial P_0}\end{pmatrix}. \quad (20)$$

Here, $\mathbf{W}(t)$ is the standard monodromy matrix from classical mechanics.

Next, in the case that multiple trajectories evolve to (R,P) at time t, denote the original positions of the particles at time $t=0$ by $(\tilde{R}_0^k,\tilde{P}_0^k)$ and their electronic density matrices at time t by $\tilde{\boldsymbol{\sigma}}^k(t)$. In this case, according to Eq. (19), we find

$$A_{ij}^{\mathrm{MF}}(R,P,t) = \sum_k \frac{f(\tilde{R}_0^k,\tilde{P}_0^k)\tilde{\boldsymbol{\sigma}}^k(t)}{|\det(\mathbf{W}(\tilde{R}_0^k,\tilde{P}_0^k,t))|}. \tag{21}$$

This completes our prescription for constructing $\mathbf{A}^{\mathrm{MF}}(R,P,t)$.

Unfortunately, as written in Eq. (21), an equation of motion does not exist for $A_{ij}^{\mathrm{MF}}(R,P,t)$, in general. The problem is that, according to Eq. (21), knowledge of $A_{ij}^{\mathrm{MF}}(R,P,t)$ for all (R,P) does not imply complete information about all individual trajectories. In particular, when two trajectories reach the same classical coordinates (R,P) at time t, the trajectory information is averaged to yield $A_{ij}^{\mathrm{MF}}(R,P,t)$. For this reason, knowledge of $A_{ij}^{\mathrm{MF}}(R,P)$ at time t is not enough to predict the probability distribution at time $t+\Delta t$. This inability to define an equation of motion for the probability distribution can be considered a deficiency of our Ehrenfest approach. After all, an equation of motion for the true joint nuclear-electronic probability does exist within the rigorous framework of a partial Wigner transform.

Notwithstanding this formal difficulty, when the swarm of trajectories happens to evolve such that no two trajectories ever reach the same classical coordinates (R,P) at time t, then there is an equation of motion for A_{ij}^{MF}. In this case, Eq. (20) is always applicable, and the swarm of particles evolves much like a classical fluid undergoing Hamiltonian dynamics, only with the extra complication that nuclear motion remains coupled to the electronic state of the system. For the remainder of this paper, we will always invoke this *unique preimage* assumption: we assume that at time t, the phase space point (R,P) has exactly *one* preimage from the swarm of trajectories at time $t=0$. If every trajectory begins in the same initial electronic state at time $t=0$, this assumption must be valid for short times. In general, we expect this approximation to fail at long times; at such times, we also expect that standard Ehrenfest dynamics will be inaccurate.

In order to derive an equation of motion, let us define at time t,

$$f(R,P,t) \equiv \mathrm{Tr}(\mathbf{A}(R,P,t)), \tag{22}$$

$$\boldsymbol{\sigma}(R,P,t) \equiv \mathbf{A}^{\mathrm{MF}}(R,P,t)/f(R,P,t), \tag{23}$$

so that $A_{ij}^{\mathrm{MF}}(R,P,t)=f(R,P,t)\sigma_{ij}(R,P,t)$. If we now invoke the unique preimage assumption, it follows that $\boldsymbol{\sigma}(R,P,t)$ is the electronic density matrix associated with the nucleus at position (R,P) and $\boldsymbol{\sigma}$ evolves according to Eq. (9).

We now have all of the necessary tools to derive an equation of motion. If we take the partial derivative of $A_{ij}^{\mathrm{MF}}(R,P,t)=f(R,P,t)\sigma_{ij}(R,P,t)$ with respect to time, we find

$$\frac{\partial A_{ij}^{\mathrm{MF}}(R,P,t)}{\partial t} = \frac{\partial f(R,P,t)}{\partial t}\sigma_{ij}(R,P,t) + f(R,P,t)\frac{\partial \sigma_{ij}(R,P,t)}{\partial t}. \tag{24}$$

The term $\partial\sigma_{ij}(R,P,t)/\partial t$ in Eq. (24) may be evaluated using the identity

$$\frac{d\sigma_{ij}(R,P,t)}{dt} = \frac{\partial\sigma_{ij}(R,P,t)}{\partial t} + \frac{\partial\sigma_{ij}(R,P,t)}{\partial R}\dot{R} + \frac{\partial\sigma_{ij}(R,P,t)}{\partial P}\dot{P}, \tag{25}$$

together with the equations of motion for $d\sigma_{ij}/dt$, $\dot{R}$, and $\dot{P}$ [Eqs. (9)–(11)], leading to

$$\begin{aligned}\frac{\partial\sigma_{ij}(R,P,t)}{\partial t} =& -\frac{i}{\hbar}\sum_k (H_{ik}^{\mathrm{el}}\sigma_{kj} - \sigma_{ik}H_{kj}^{\mathrm{el}}) \\ & - \frac{P}{M}\sum_k (d_{ik}(R)\sigma_{kj} - \sigma_{ik}d_{kj}(R)) \\ & - \frac{\partial\sigma_{ij}(R,P,t)}{\partial R}\frac{P}{M} \\ & + \frac{\partial\sigma_{ij}(R,P,t)}{\partial P}\left(\sum_{kl} F_{kl}(R)\sigma_{lk}(R,P,t)\right).\end{aligned} \tag{26}$$

Furthermore, the term $\partial f(R,P,t)/\partial t$ in Eq. (24) may be evaluated using the continuity equation for the density of the classical nucleus,

$$\frac{\partial f(R,P,t)}{\partial t} = -\frac{\partial}{\partial R}(f(R,P,t)\dot{R}) - \frac{\partial}{\partial P}(f(R,P,t)\dot{P}) \tag{27}$$

$$= -\frac{\partial f(R,P,t)}{\partial R}\dot{R} - \frac{\partial f(R,P,t)}{\partial P}\dot{P} - f(R,P,t)\frac{\partial\dot{P}}{\partial P} \tag{28}$$

$$\begin{aligned}=& -\frac{\partial f(R,P,t)}{\partial R}\frac{P}{M} + \frac{\partial f(R,P,t)}{\partial P}\left(\sum_{ij} F_{ij}\sigma_{ji}\right) \\ & + f(R,P,t)\left(\sum_{kl}\frac{\partial\sigma_{kl}(t)}{\partial P}F_{lk}(R)\right).\end{aligned} \tag{29}$$

Altogether, using $\mathbf{A}^{\mathrm{MF}}=f\boldsymbol{\sigma}$ and Eqs. (24), (25), and (29), we find that the equation of motion for the probability density $A_{ij}^{\mathrm{MF}}(R,P,t)$ is

$$\begin{aligned}\frac{\partial}{\partial t}A_{ij}^{\mathrm{MF}}(R,P,t) =& -\frac{i}{\hbar}\left(\sum_k H_{ik}^{\mathrm{el}}(R)A_{kj}^{\mathrm{MF}}(t) - A_{ik}^{\mathrm{MF}}(t)H_{kj}^{\mathrm{el}}(R)\right) \\ & - \frac{P}{M}\sum_k (d_{ik}(R)A_{kj}^{\mathrm{MF}}(t) - A_{ik}^{\mathrm{MF}}(t)d_{kj}(R)) \\ & - \frac{P}{M}\frac{\partial A_{ij}^{\mathrm{MF}}(t)}{\partial R} + \left(\sum_{kl}\sigma_{kl}(t)F_{lk}(R)\right)\frac{\partial A_{ij}^{\mathrm{MF}}(t)}{\partial P} \\ & + \left(\sum_{kl}\frac{\partial\sigma_{kl}(t)}{\partial P}F_{lk}(R)\right)A_{ij}^{\mathrm{MF}}(t).\end{aligned} \tag{30}$$

Equation (30) is the formal equation of the motion for the mean-field probability density. As emphasized above, the matrix $\sigma_{kl}(t)$ that appears on the right hand side must be understood as the unique electronic density matrix corresponding to point (R,P) under the unique preimage assumption. Note the similarities between Eqs. (30) and (18); this will be explored in Sec. IV.

Before completing this section, we mention that the last term in Eq. (28) is equal to zero for standard Hamiltonian

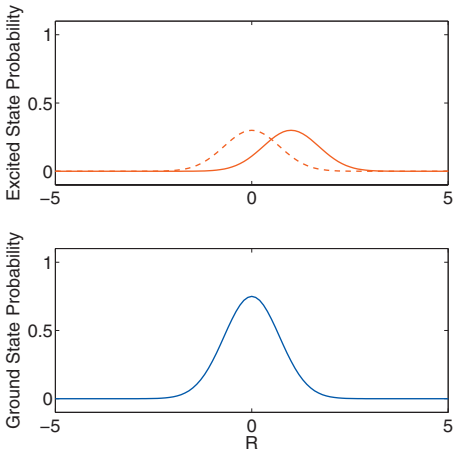

FIG. 1. The relative positions of nuclear wave packets on different potential energy surface are partially described by the mixed nuclear-electronic derivatives, $\partial A_{ij}/\partial P$ and $\partial A_{ij}/\partial R$. Here, we plot in blue a nuclear wave packet on the ground state. The corresponding wave packet on the excited state is drawn red: the line is dashed if the wave packets are vertically aligned and full if there is a displacement between the two (the latter sometimes leading to decoherence). Standard Ehrenfest dynamics carries no information about this shift in the nuclear position with respect to the electronic state—it quantifies only the relative populations on the different potential energy surfaces.

dynamics, where $\dot{P}$ depends only on the position, $\dot{P}=-V'(R)$. For Ehrenfest dynamics, however, this is not so. According to Eq. (11), $\dot{P}$ depends on $\boldsymbol{\sigma}$, which, in turn, depends on P, so this term is not zero [which leads to the final term in Eq. (29)]. We must conclude therefore that, according to Eq. (28), during Ehrenfest dynamics—and unlike Hamiltonian dynamics—the probability density for a nucleus can change along a trajectory,

$$\frac{df(R,P,t)}{dt} = \frac{\partial f(R,P,t)}{\partial t} + \frac{\partial f(R,P,t)}{\partial R}\dot{R} + \frac{\partial f(R,P,t)}{\partial P}\dot{P} \quad (31)$$

$$= -f(R,P,t)\frac{\partial \dot{P}}{\partial P} \quad (32)$$

$$= f(R,P,t)\left(\sum_{kl}\frac{\partial \sigma_{kl}(t)}{\partial P}F_{lk}(R)\right). \quad (33)$$

This implies that, in general, $|\det(\mathbf{W})| \neq 1$ in Eq. (20).

B. Computing the partial derivatives $\partial A_{ij}/\partial P$, $\partial A_{ij}/\partial R$

In Sec. IV, we will exploit the similarities between Eqs. (18) and (30). Before doing so, however, we now show how the matrix elements $\partial A_{ij}/\partial P$ and $\partial A_{ij}/\partial R$ may be computed along an Ehrenfest trajectory during a practical calculation. These mixed nuclear-electronic derivatives give information about the relative shift in positions between nuclear wave packets on different potential energy surfaces (see Fig. 1).

Recall that, under the unique preimage assumption, we may write

$$A_{ij}^{\mathrm{MF}}(R,P,t) = f(R,P,t)\sigma_{ij}(R,P,t), \quad (34)$$

where $\sigma_{ij}(R,P,t)$ evolves according to Eq. (9) and $f(R,P,t)$ satisfies the continuity equation [Eq. (27)]. Taking partial derivatives of both sides, it follows that

$$\frac{\partial A_{ij}^{\mathrm{MF}}(R,P,t)}{\partial R} = \frac{\partial f(R,P,t)}{\partial R}\sigma_{ij}(R,P,t) + f(R,P,t)\frac{\partial \sigma_{ij}(R,P,t)}{\partial R}, \quad (35)$$

$$\frac{\partial A_{ij}^{\mathrm{MF}}(R,P,t)}{\partial P} = \frac{\partial f(R,P,t)}{\partial P}\sigma_{ij}(R,P,t) + f(R,P,t)\frac{\partial \sigma_{ij}(R,P,t)}{\partial P}. \quad (36)$$

By treating the nucleus classically, we may safely assume that, at time $t=0$, the particle sits at the center of a distribution in phase space, much like the center of a Gaussian,

$$\frac{\partial f(R,P,0)}{\partial R} = \frac{\partial f(R,P,0)}{\partial P} = 0. \quad (37)$$

In theory, we could propagate the derivatives $\partial f/\partial R$ and $\partial f/\partial P$ using Eq. (33) and the identities

$$\frac{d}{dt}\frac{\partial f}{\partial R} = \frac{\partial}{\partial R}\frac{df}{dt} - \frac{\partial f}{\partial P}\frac{\partial \dot{P}}{\partial R}, \quad (38)$$

$$\frac{d}{dt}\frac{\partial f}{\partial P} = \frac{\partial}{\partial P}\frac{df}{dt} - \frac{1}{M}\frac{\partial f}{\partial R}. \quad (39)$$

As a practical matter, however, we will show that such derivatives of f are usually unnecessary.

According to Eqs. (35) and (36), it remains only to calculate the derivatives $\partial \sigma_{ij}/\partial R$ and $\partial \sigma_{ij}/\partial P$. This is done in Appendix B. For maximum generality, we report the results for arbitrarily many nuclear coordinates. Recall that nuclear coordinates are denoted by superscript Greek indices, and electronic coordinates are denoted by subscript Roman indices,

$$\begin{aligned}\frac{d}{dt}\frac{\partial \sigma_{rs}}{\partial R^{\beta}} =& -\frac{i}{\hbar}\sum_{k}\left(H_{rk}(R)\frac{\partial \sigma_{ks}}{\partial R^{\beta}} - \frac{\partial \sigma_{rk}}{\partial R^{\beta}}H_{ks}(R)\right)\\ &-\frac{i}{\hbar}\sum_{k}\left(F_{rk}^{\beta}(R)\sigma_{ks} - \sigma_{rk}F_{ks}^{\beta}(R)\right)\\ &-\sum_{\alpha k}\frac{P^{\alpha}}{M}\left(d_{rk}^{\alpha}(R)\frac{\partial \sigma_{ks}}{\partial R^{\beta}} - \frac{\partial \sigma_{rk}}{\partial R^{\beta}}d_{ks}^{\alpha}(R)\right)\\ &-\sum_{\alpha k}\frac{P^{\alpha}}{M}\left(\frac{\partial d_{rk}^{\alpha}(R)}{\partial R^{\beta}}\sigma_{ks} - \sigma_{rk}\frac{\partial d_{ks}^{\alpha}(R)}{\partial R^{\beta}}\right)\\ &+\sum_{\alpha kl}\frac{\partial \sigma_{rs}}{\partial P^{\alpha}}\frac{\partial \sigma_{kl}}{\partial R^{\beta}}F_{lk}^{\alpha}(R) + \sum_{\alpha kl}\frac{\partial \sigma_{rs}}{\partial P^{\alpha}}\sigma_{kl}\frac{\partial F_{lk}^{\alpha}}{\partial R^{\beta}}(R),\end{aligned} \quad (40)$$

$$\frac{d}{dt}\frac{\partial \sigma_{rs}}{\partial P^{\beta}} = -\frac{i}{\hbar}\sum_{k}\left(H_{rk}(R)\frac{\partial \sigma_{ks}}{\partial P^{\beta}} - \frac{\partial \sigma_{rk}}{\partial P^{\beta}}H_{ks}(R)\right) - \sum_{\alpha k}\frac{P^{\alpha}}{M}\left(d^{\alpha}_{rk}(R)\frac{\partial \sigma_{ks}}{\partial P^{\beta}} - \frac{\partial \sigma_{rk}}{\partial P^{\beta}}d^{\alpha}_{ks}(R)\right) - \frac{1}{M}\sum_{k}\left(d^{\beta}_{rk}(R)\sigma_{ks} - \sigma_{rk}d^{\beta}_{ks}(R)\right) - \frac{1}{M}\frac{\partial \sigma_{rs}}{\partial R^{\beta}} + \sum_{\alpha kl}\frac{\partial \sigma_{rs}}{\partial P^{\alpha}}\frac{\partial \sigma_{kl}}{\partial P^{\beta}}F^{\alpha}_{lk}(R). \quad (41)$$

Armed with Eqs. (35), (36), (40), and (41), we have provided a complete description for calculating approximately the instantaneous equation of motion for the mean-field probability density [Eq. (30)] along a propagated Ehrenfest trajectory. In Sec. IV, we show how this formalism may be applied to understand decoherence and the failures of standard Ehrenfest dynamics.

IV. THEORY: NONADIABATIC MEAN-FIELD DYNAMICS WITH STOCHASTIC DECOHERENCE

A. Combining the mean-field and partial Wigner descriptions

Suppose that at time t the mean-field and partial Wigner transform probability densities agree $\mathbf{A}^{\mathrm{MF}}(R,P,t) = \mathbf{A}^{W}(R,P,t)$ everywhere in phase space. Comparing Eqs. (18) and (30), the straightforward conclusion is that, at position (R,P) in phase space, the ijth element of the two probability densities are diverging at the (complex) rate

$$\Gamma_{ij} = \sum_{kl}(F_{kl}(R)\sigma_{lk})\frac{\partial A_{ij}}{\partial P} + \sum_{kl}\left(F_{kl}(R)\frac{\partial \sigma_{lk}}{\partial P}\right)A_{ij} - \frac{1}{2}\sum_{k}\left(F_{ik}(R)\frac{\partial A_{kj}}{\partial P} + \frac{\partial A_{ik}}{\partial P}F_{kj}(R)\right). \quad (42)$$

Thus, calculating Eq. (42) is a means to check the accuracy of standard Ehrenfest dynamics along a single trajectory.

As mentioned in Sec. II, many physical effects lead to the difference in time propagation between Ehrenfest and partial Wigner transform dynamics, as encapsulated by Γ_{ij}. The most importance difference is that partial Wigner transform dynamics allow for nuclear wave packets on different adiabatic surfaces to feel different forces and separate, while Ehrenfest dynamics do not. Beyond separation on different adiabatic states, the MF wave packet and the nuclear wave packet on electronic state i should also move apart in space. All of these effects are encapsulated in the rate Γ_{ij}. Mathematically, as $t\to\infty$, we expect that $|A^{\mathrm{MF}}_{ii}(R,P,t) - A^{W}_{ii}(R,P,t)|\to 0$ and $|A^{W}_{ij}|\to 0$ $(i\neq j)$ even though A^{MF}_{ij} does not usually converge to 0. For these reasons, Schwartz and co-workers[13,14] predicted that Ehrenfest dynamics could be corrected by introducing stochastic decoherence events. We will presently explore how we may extract a rate for such decoherence from Eqs. (18), (30), and (42).

B. A rate for decoherence

As recognized by all nonadiabatic surface-hopping algorithms, the rate of decoherence and collapse to a specific electronic state $|\Phi_k\rangle$ (denoted by γ_k) should be proportional to (i) the instantaneous electronic population on state k, σ_{kk}, and (ii) the simulation time step, dt. Thus, we can always write

$$\gamma_k = \frac{\sigma_{kk}}{\tau}dt. \quad (43)$$

The essential piece of any surface-hopping or stochastic mean-field algorithm is choosing $1/\tau$, the rate of decoherence. (Note that, for the Schwartz algorithm, there is no unique $1/\tau$, but rather a set of $\{1/\tau_k\}$, one for each state k.) In order to derive an approximate $1/\tau$, we will take two different intuitive approaches starting with Eqs. (18) and (30) and show that they yield very similar final answers [Eqs. (46) and (52)]. Afterward, we will show that Eq. (52) can also be derived independently using a frozen Gaussian interpretation of Ehrenfest dynamics. In Sec. VI, we will demonstrate that our computed decoherence rate performs well for the Tully model problems.

1. Heuristic approach: Γ as a "decoherence operator"

If we view Eq. (42) as arising primarily from the failure of the Ehrenfest dynamics to allow decoherence, then the most simple expression for a decoherence rate would be to treat the matrix Γ in Eq. (42) as an operator and take its expectation value. Using the unique preimage assumption, we may write $A_{ij}=f\sigma_{ij}$ and then evaluate the decoherence rate $(1/\tau_d)$ as the expectation value with respect to $\boldsymbol{\sigma}$,

$$\frac{1}{\tau_d} \propto |\mathrm{Tr}(\boldsymbol{\Gamma}\boldsymbol{\sigma})| = \left|\sum_{kl}\Gamma_{kl}\sigma_{lk}\right|. \quad (44)$$

Plugging into Eq. (42) and using the fact that the density matrix is pure until decoherence $(\boldsymbol{\sigma}^2=\boldsymbol{\sigma})$, we find that the expression simplifies greatly, eliminating any dependence on the factor $\partial f/\partial P$, leaving

$$\frac{1}{\tau_d} \propto \frac{f}{2}\left|\sum_{ij}F_{ij}\frac{\partial \sigma_{ji}}{\partial P}\right|. \quad (45)$$

In order for τ_d to have the correct units (of time), Eq. (45) must divided by the density of the particle swarm in phase space. The obvious choice is f, leading us to

$$\frac{1}{\tau_d} \approx \frac{1}{2}\left|\sum_{ij}F_{ij}\frac{\partial \sigma_{ji}}{\partial P}\right|. \quad (46)$$

Equation (46) represents our first and most naive approach for computing a decoherence rate. We can do better.

2. A decoherence rate as a depurification

A similar, but more refined, expression for the decoherence rate at time t can be constructed by considering the purity of the instantaneous density matrix (which exists under the unique preimage assumption),

$$Y = \mathrm{Tr}(\boldsymbol{\sigma} - \boldsymbol{\sigma}^2) = \sum_i \sigma_{ii} - \sum_{ij} \sigma_{ij}\sigma_{ji} = 1 - \sum_{ij} \sigma_{ij}\sigma_{ji}. \quad (47)$$

When $Y=0$, we are in a pure state, and when $Y=1/2$, we are in a completely mixed state.

Let us assume that the Ehrenfest and partial Wigner probability densities are instantaneously equal at time t, and we write $A_{ij}^W = A_{ij}^{\mathrm{MF}} = f\sigma_{ij}$. Let us further assume that we are near the center of a nuclear wave packet where $\partial f/\partial R = \partial f/\partial P = 0$, and that the dynamics in phase space will be incompressible so that $\partial f/\partial t = 0$. If we now follow partial Wigner dynamics, we find

$$f\frac{\partial}{\partial t}\sigma_{ij}(R,P,t) = \frac{-if}{\hbar}\left(\sum_k H_{ik}^{\mathrm{el}}(R)\sigma_{kj} - \sigma_{ik}H_{kj}^{\mathrm{el}}(R)\right) - \sum_k \frac{fP}{M}(d_{ik}(R)\sigma_{kj} - \sigma_{ik}d_{kj}(R)) - \frac{fP}{M}\frac{\partial \sigma_{ij}}{\partial R} + \frac{f}{2}\sum_k \left(F_{ik}(R)\frac{\partial \sigma_{kj}}{\partial P} + \frac{\partial \sigma_{ik}}{\partial P}F_{kj}(R)\right). \quad (48)$$

Defining the decoherence rate $(1/\tau_d)$ as the rate at which $\boldsymbol{\sigma}$ loses its purity, we find that many terms in Eq. (48) cancel or have zero contribution, and there is a simple expression

$$1/\tau_d = \frac{\partial}{\partial t}Y \quad (49)$$

$$= -2\sum_{ij}\left(\frac{\partial}{\partial t}\sigma_{ij}\right)\sigma_{ji} \quad (50)$$

$$= -\sum_{ij} F_{ij}\frac{\partial \sigma_{ji}}{\partial P}. \quad (51)$$

Equation (51) is very similar to Eq. (46), only now without absolute value signs and a factor of 2. The absence of absolute value signs in Eq. (51) reflects the fact that the density matrix can instantaneously increase or decrease its purity. Because decoherence is the rate of depurification, we want only the positive piece of Eq. (51). Thus, from this perspective, the optimal choice of the decoherence rate is

$$\frac{1}{\tau_d} = \max\left(0, -\sum_{ij} F_{ij}\frac{\partial \sigma_{ji}}{\partial P}\right), \quad (52)$$

which can be extended to the case of many nuclear degrees of freedom as

$$\frac{1}{\tau_d} = \max\left(0, -\sum_{ij\beta} F_{ij}^{\beta}\frac{\partial \sigma_{ji}}{\partial P^{\beta}}\right). \quad (53)$$

3. A frozen Gaussian interpretation

A frozen Gaussian[38] interpretation of Ehrenfest dynamics confirms our intuitive derivation of Eq. (52) above. Consider a set of normalized Gaussian wave packets with centers $R_i(t)$ in real space and $P_i(t)$ in momentum space, and widths a_R and $a_P = \hbar/a_R$,

$$g_i(R) \equiv \langle R|g_i(R_i,P_i)\rangle \equiv \left(\frac{1}{\pi a_R^2}\right)^{1/4}\exp\left(\frac{-(R-R_i(t))^2}{2a_R^2}\right) \times \exp\left(\frac{i}{\hbar}P_i(t)(R-R_i(t))\right), \quad (54)$$

$$g_i(P) \equiv \langle P|g_i(R_i,P_i)\rangle \equiv \left(\frac{1}{\pi a_P^2}\right)^{1/4}\exp\left(\frac{-(P-P_i(t))^2}{2a_P^2}\right) \times \exp\left(-\frac{i}{\hbar}PR_i(t)\right). \quad (55)$$

The overlap between a pair of such Gaussian wave packets is exactly[39,40]

$$\langle g_i|g_j\rangle = \exp\left(\frac{-1}{4a_R^2}(R_i(t)-R_j(t))^2\right)\exp\left(\frac{-1}{4a_P^2}(P_i(t)-P_j(t))^2\right) \times \exp\left(\frac{i}{2\hbar}(R_i(t)-R_j(t))(P_i(t)+P_j(t))\right). \quad (56)$$

As noted many times before (e.g., Ref. 38), the centers of frozen Gaussian wave packets move according to classical mechanics for short times

$$R_i(t) = R_i(0) + \frac{P_i(0)}{M}t, \quad (57)$$

$$P_i(t) = P_i(0) - F_i(0)t, \quad (58)$$

where, as usual, we have defined F as the negative of the conventional force in Eq. (58). To first order in time t, according to Eqs. (56)–(58), we find

$$|\langle g_i|g_j\rangle| = \exp\left(\frac{-1}{2Ma_R^2}(R_i(0)-R_j(0))(P_i(0)-P_j(0))t\right) \times \exp\left(\frac{1}{2a_P^2}(P_i(0)-P_j(0))(F_i(0)-F_j(0))t\right).$$

Thus, ignoring phase, we find that the frozen Gaussian wave packets move apart instantaneously at the rate

$$\frac{1}{\tilde{\tau}_d} = \frac{(R_i(0)-R_j(0))(P_i(0)-P_j(0))}{2Ma_R^2} - \frac{(P_i(0)-P_j(0))(F_i(0)-F_j(0))}{2a_P^2}. \quad (59)$$

Moreover, if g_i has probability $|c_i|^2$ to be occupied and g_j has probability $|c_j|^2$ to be occupied, then the probability to find two particles at the same point in phase space is decreasing roughly at the rate

$$\frac{1}{\tau_d} = |c_i|^2|c_j|^2\left(\frac{(R_i(0)-R_j(0))(P_i(0)-P_j(0))}{Ma_R^2} - \frac{(P_i(0)-P_j(0))(F_i(0)-F_j(0))}{a_P^2}\right). \quad (60)$$

Let us now interpret an Ehrenfest wave packet with classical coordinates $\bar{R}$ and $\bar{P}$ as being the coherent sum of two Gaussian wave packets, g_1 and g_2, on electronic surfaces $\Phi_1(R)$ and $\Phi_2(R)$, with coefficients c_1 and c_2,

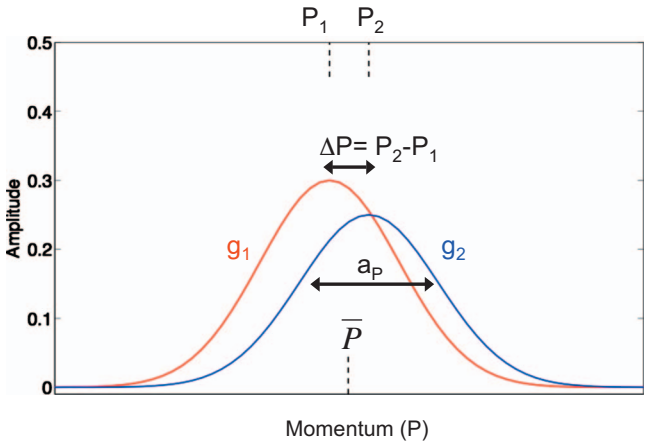

FIG. 2. According to our interpretation of augmented Ehrenfest dynamics, the "Ehrenfest wave function" represents two frozen Gaussians g_1 and g_2, with different centers R_1, P_1 and R_2, P_2 in phase space. The Ehrenfest variables, $\bar{R}$ and $\bar{P}$, satisfy $\bar{R}=|c_1|^2R_1+|c_2|^2R_2$ and $\bar{P}=|c_1|^2P_1+|c_2|^2P_2$, where $|c_1|^2, |c_2|^2$ are the probabilistic weights of the different frozen Gaussians. The decoherence captured by Eqs. (52) and (71) represents the rate at which these wave packets move apart. In this figure, we plot the shift in momentum space only.

$$\Psi_{\text{Ehrenfest}}(r,R) = c_1\Phi_1(r;R)g_1(R) + c_2\Phi_2(r;R)g_2(R). \tag{61}$$

We will assume that $\bar{R}$ and $\bar{P}$ are the mean wave packet centers

$$\bar{R} = |c_1|^2R_1 + |c_2|^2R_2, \tag{62}$$

$$\bar{P} = |c_1|^2P_1 + |c_2|^2P_2 \tag{63}$$

(see Fig. 2). We define $\Delta R=R_2-R_1$ and $\Delta P=P_2-P_1$.

With this interpretation, the dimensionless $\boldsymbol{\sigma}$ matrix in Ehrenfest dynamics is

$$\boldsymbol{\sigma} = \sqrt{\pi a_R^2}\begin{pmatrix} |c_1|^2|g_1|^2 & c_1c_2^*g_1g_2^* \\ c_2c_1^*g_2g_1^* & |c_2|^2|g_2|^2 \end{pmatrix}, \tag{64}$$

which is normalized so that $\sigma_{11}+\sigma_{22}\approx 1$, assuming that $\Delta P \ll a_P$ and $\Delta R \ll a_R$. It follows that

$$\begin{aligned}\left.\frac{\partial\sigma_{11}}{\partial P}\right|_{P=\bar{P}} &= |c_1|^2 \left.\frac{\partial\left(\exp\left(\frac{-(P-P_1)^2}{a_P^2}\right)\right)}{\partial P}\right|_{P=\bar{P}} \\ &= -2|c_1|^2\frac{(\bar{P}-P_1)}{a_P^2}\exp\left(\frac{-(\bar{P}-P_1)^2}{a_P^2}\right) \\ &\approx -2|c_1|^2|c_2|^2\frac{(P_2-P_1)}{a_P^2} \\ &= -2|c_1|^2|c_2|^2\frac{\Delta P}{a_P^2} \\ &\approx -\left.\frac{\partial\sigma_{22}}{\partial P}\right|_{P=\bar{P}}.\end{aligned} \tag{65, 66}$$

The equivalent expression for real space is also true

$$\begin{aligned}\left.\frac{\partial\sigma_{11}}{\partial R}\right|_{R=\bar{R}} &\approx -2|c_1|^2|c_2|^2\frac{\Delta R}{a_R^2} \\ &= -2|c_1|^2|c_2|^2\frac{\Delta R a_P^2}{\hbar^2} \\ &\approx -\left.\frac{\partial\sigma_{22}}{\partial R}\right|_{R=\bar{R}}.\end{aligned} \tag{67}$$

Using the analysis above, our final result is that the second term in Eq. (60) matches our earlier expressions for a decoherence rate (up to a factor of 1/2)

$$\frac{1}{\tau_d}(\text{Term } 2) = -\frac{(P_2-P_1)(F_2(0)-F_1(0))}{a_P^2}|c_1|^2|c_2|^2 \tag{68}$$

$$\approx -\frac{1}{2}\left(F_{11}\frac{\partial\sigma_{11}}{\partial P} + F_{22}\frac{\partial\sigma_{22}}{\partial P}\right) \tag{69}$$

$$\approx -\frac{1}{2}\sum_{ij}F_{ij}\frac{\partial\sigma_{ji}}{\partial P}. \tag{70}$$

Unfortunately, unlike the second term, the first term in Eq. (60) cannot be expressed using the dynamic variables $\partial\boldsymbol{\sigma}/\partial P$ and $\partial\boldsymbol{\sigma}/\partial R$. Effectively, our scheme propagates two variables that are related to the decoherence of the Ehrenfest wave packet. At the same time, however, there are three unknown variables: ΔR, ΔP, and a_R, and no combination of Eq. (66) or Eq. (67) leads to the product expression $\Delta R\Delta P/a_R^2$ in Eq. (60). The best we can do is assume that the frozen Gaussian wave packets are moving away from each other with the same speed in both momentum and real space. Thus, we are led to double the decoherence rate in Eq. (52),

$$\frac{1}{\tau_d} \approx -\sum_{ij}F_{ij}\frac{\partial\sigma_{ji}}{\partial P}. \tag{71}$$

The physical meaning of the decoherence rate in Eq. (71) is as follows: when $\text{Tr}(-F\cdot(\partial\boldsymbol{\sigma}/\partial P))$ is positive, the wave packet with the more positive momentum is experiencing a more positive force than the wave packet with the less positive momentum. Thus, a positive value means that the Gaussian wave packets are moving apart and a negative value indicates that the wave packets are moving together. For this reason, we take only the positive piece of Eq. (71) in Eq. (52).

4. An empirical correction to ensure decoherence

Although we would like to choose $1/\tau_d$ shown above as our exact decoherence rate, empirically we have found that our results are enhanced by inserting a correction to the expression for τ_d above. In order to ensure that decoherence is total and irreversible, and that the wave packets separate before $\int dt/\tau_d(t)=1$, we will adjust the probability for a decoherence event in a time interval dt (per unit population) to be

$$\frac{1}{\tau(t)} = \frac{1}{\tau_d(t)} \frac{1}{1 - S(t)}, \quad S(t) = \int_{t_*}^{t} \frac{dt'}{\tau_d(t')}, \tag{72}$$

where t_* is either the infinite past or the time of the last decoherence event. Physically, this adjustment means that $\Delta t/\tau$ is roughly the fraction of the initial wave packet norm (at $t=0$) that decoheres in the window Δt; $\Delta t/\tau$ is *not* the fraction of the instantaneous wave packet norm (at time $t>0$) that decoheres in this window [see Eq. (33)].

In Sec. VI, for the set of Tully model problems, we present numerical data using $1/\tau$ as defined in Eq. (72) and show that it performs quite well. We will calculate $1/\tau_d$ according to Eq. (71) or Eq. (70) in order to show the importance of the extra factor of 2 discussed above.

C. Energy conservation and a novel treatment of forbidden hops

Energy conservation is the final, necessary ingredient for a nonadiabatic dynamics algorithm. In general, the details of how energy is conserved are somewhat *ad hoc* for any mixed quantum-classical algorithm, although there appears to be general agreement that the velocity in the direction of the instantaneous nonadiabatic derivative coupling vector is crucial. For the numerical results presented below, we have implemented a slightly unorthodox treatment to ensure energy conservation that is not always local in position space but that usually avoids "forbidden" hops. We describe this now.

Suppose that the classical particle is at position R with an average electronic potential $\langle H^{\mathrm{el}}(R)\rangle$, and we want to decohere into electronic state k. Let P_{na} be the momentum in the direction of the instantaneous nonadiabatic derivative coupling, $\vec{v}_{\mathrm{na}}=\vec{d}_{12}/|\vec{d}_{12}|$. Following the usual surface-hopping formalism we would like to conserve energy during a decoherence event by rescaling P_{na},

$$\frac{(P_{\mathrm{na}})^2}{2M} + \langle H^{\mathrm{el}}(R)\rangle = \frac{(P_{\mathrm{na}}^{\mathrm{rescale}})^2}{2M} + H_{kk}^{\mathrm{el}}(R), \tag{73}$$

As usual, however, two distinct cases present themselves.

On the one hand, there are so-called "allowed" collapses, where $(P_{\mathrm{na}})^2/2M > H_{kk}^{\mathrm{el}}(R) - \langle H^{\mathrm{el}}(R)\rangle$. This is always true, for instance, when the state k is the ground state. In this case, we follow convention and rescale P_{na} during the collapse event.

On the other hand, when k is an excited state, there are also so-called forbidden collapses, where $(P_{\mathrm{na}})^2/2M < H_{kk}^{\mathrm{el}}(R) - \langle H^{\mathrm{el}}(R)\rangle$. In this case, we do not follow the usual convention. In general, because such a collapse at point R is not energetically possible, the usual prescription is to ignore such a decoherence event. In our algorithm, we will ignore such an event only when the excited state k has never been energetically accessible.

More generally, instead of ignoring the collapse, we have chosen to (i) reverse the dynamical Ehrenfest trajectory in time, moving (R,P) backward to the last point in phase space where electronic state k was energetically accessible, and then (ii) collapse the wave function at that new point with the momentum correctly rescaled to conserve energy (see Fig. 3). In this sense, we do not ignore forbidden hops.

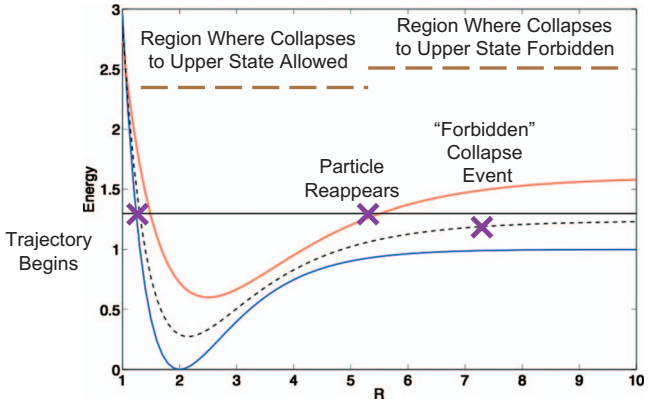

FIG. 3. An energy diagram showing how forbidden hops are avoided. Here, the ground state energy is colored blue, the first excited state energy is colored red, and the mean-field energy is a dotted black line. The total energy of the system is the solid black line at $E=1.3$. In this case, an Ehrenfest trajectory begins in the ground state at $R=1.2$ with positive momentum and, as the particle moves forward, it quickly begins to experience a mixed, mean-field force. At position $R=5.3$, the upper state becomes energetically inaccessible. At position $R=7.5$, as the particle continues on a mean-field surface, a collapsing event occurs. If the collapse is to the upper state, the particle reappears at position $R=5.3$ in the upper state with a new momentum that has been rescaled to ensure energy conservation.

We will show in Sec. VI that this nonlocal treatment of forbidden hops is a key ingredient for solving the third Tully model problem correctly. A similar scheme can also be found in Ref. 9.

Finally, as a matter of computational efficiency, note that one does not ever need to run Ehrenfest dynamics backward in time for an actual calculation. An equivalent technique is to calculate the rescaled momenta at every point along a trajectory and save this information in memory. Then, on the chance that a forbidden hop may occur in the future, one already knows the correct coordinates for the decoherence event and one never needs to go backward. We have implemented this latter trick for our numerical examples below.

V. STEP-BY-STEP ALGORITHMIC OUTLINE

For completeness, we now give a step-by-step outline of the algorithm above for performing nonadiabatic dynamics.

(1) Initialize the mixed quantum-classical trajectory by fixing the initial classical coordinates (R_0,P_0) and electronic density matrix $\boldsymbol{\sigma}_0$ at time $t=0$. To simulate a classical nucleus at time $t=0$ with a well-defined electronic state, set also $\partial\boldsymbol{\sigma}_{ij}(R_0,P_0,0)/\partial R = \partial\boldsymbol{\sigma}_{ij}(R_0,P_0,0)/\partial P = 0$. Set R_{save} and P_{save} to NULL, and set $S(0)=0$. [S is defined in Eq. (72).]

(2) Between time t and $t+dt$, propagate $\boldsymbol{\sigma}$, R, P, $\partial\boldsymbol{\sigma}/\partial R$, and $\partial\boldsymbol{\sigma}/\partial P$ according to Eqs. (9)–(11), (40), and (41), respectively. For the numerical examples below, we have performed this integration with fourth-order Runge–Kutta.

(3) Set $t=t+dt$ and evaluate the rate $1/\tau_d(t)$ in Eq. (52).

(4) Update $S(t)=S(t-dt)+dt/\tau_d(t)$. Calculate $1/\tau(t)$ according to Eq. (72). Compute the decoherence probabilities γ_1 and γ_2 [Eq. (43)].

(5) Check whether the upper state is energetically accessible according to Eq. (73).

(a) If the upper state is not accessible, continue to step (6).
(b) If the upper state is accessible, construct the scaled momentum that satisfies Eq. (73). Save the current position $R_{\text{save}}=R$ and the scaled momentum $P_{\text{save}}=P^{\text{rescale}}$ in memory.

(6) Use a random number generator to construct a random number $\zeta \in [0,1]$.
(7) If $\zeta > dt/\tau$, there is no stochastic decoherence event. Return to step (2).
(a) If $\zeta < \sigma_{00} dt/\tau$, there is a stochastic decoherence event to the ground state. This is always energetically allowed. Proceed to step (8).
(b) If $dt/\tau > \zeta > \sigma_{00} dt/\tau$, there is a stochastic decoherence event to the excited state. Calculate according Eq. (73) whether this decoherence event is energetically allowed or not.
(i) If accessible, proceed to step (8).
(ii) If not accessible and R_{save} and P_{save} are *not* initialized, the step is forbidden. Return to step (2).
(iii) If not accessible and R_{save} and P_{save} *are* initialized, proceed to step (9).

(8) The energetically allowed decoherence event is chosen to be vertical in position space.
(a) R is unchanged.
(b) P is rescaled according to Eq. (73) to conserve energy.
(c) Go to step (10).

(9) The energetically forbidden decoherence event is allowed only when diagonal in position space. Thus, move the particle "backward in time" by recalling the saved coordinates.
(a) Set $R=R_{\text{save}}$ and $P=P_{\text{save}}$.
(b) Go to step (10).

(10) Set $\boldsymbol{\sigma}$ to equal either $\left(\begin{smallmatrix}1 & 0\\ 0 & 0\end{smallmatrix}\right)$ or $\left(\begin{smallmatrix}0 & 0\\ 0 & 1\end{smallmatrix}\right)$, as if the electronic state had been measured.
Set also $\partial\boldsymbol{\sigma}/\partial R=\partial\boldsymbol{\sigma}/\partial P=\left(\begin{smallmatrix}0 & 0\\ 0 & 0\end{smallmatrix}\right)$ and $S(t)=0$.
(11) Return to step (2).

VI. CHEMICAL EXAMPLES: THE THREE TULLY PROBLEMS

In order to test the nonadiabatic algorithm above, we present numerical data for the three model problems suggested by Tully in his seminal paper from 1990 on FSSH.[5] All three problems have one nuclear dimension and two electronic states. One imagines that a particle is incoming on the lower electronic state and one seeks to calculate, for each outgoing channel, the probability that the particle exits into that channel (i.e., the branching ratios). These model problems will serve as strong tests of our decoherence algorithm because the mean-field approximation does not provide accurate solutions here and it fails qualitatively for the third problem. One criterion for assessing the quality of our algorithm will be whether or not we find electronic density in closed channels, which is one of the major flaws of standard Ehrenfest dynamics.

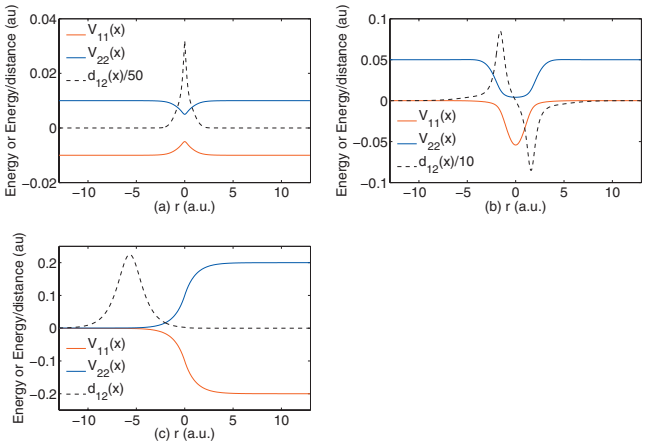

FIG. 4. The potential energy surfaces corresponding to the three Tully model problems: (a) a single avoided crossing [Eqs. (74)–(76)], (b) a dual avoided crossing [Eqs. (77)–(79)], and (c) an extended crossing [Eqs. (80)–(82)].

In Secs. VIA–VIC, we compare our results using Eqs. (52) and (72) versus results from Tully's FSSH algorithm and also versus exact quantum mechanical scattering results. Note that we have calculated the "exact" quantum mechanical results using a very crude grid-based approach, as described in Appendix A, and we estimate that our exact branching ratios are correct to within 1% or so. For completeness, we also provide results using only Ehrenfest dynamics in all data plots. In order to investigate the effect of the extra factor of 2 discussed above, we give results for τ_d using either Eq. (71) or Eq. (70).

All semiclassical calculations started with the particle at position $x=-20$ and used a time step $dt=0.3$ a.u. for dynamical propagation. Trajectories were stopped when the particle reached $x=\pm 25$. We ignored all trajectories that required more than 500 000 times steps, which was always less than 0.5% of the total.

A. Simple avoided crossing

The first model problem is a simple avoided crossing algorithm, where the diabatic curves are

$$V_{11}(x)=\begin{cases} A(1-e^{-Bx}), & x>0 \\ -A(1-e^{Bx}), & x<0, \end{cases} \tag{74}$$

$$V_{22}(x)=-V_{11}(x), \tag{75}$$

$$V_{12}(x)=V_{21}(x)=Ce^{-Dx^2}, \tag{76}$$

Here, $A=0.01$, $B=1.6$, $C=0.005$, and $D=1.0$, and the adiabatic curves are plotted in Fig. 4(a). According to energy conservation, after starting on the lower surface, the particle needs an initial k-vector satisfying $k>8.94$ a.u. in order to end up on the upper surface. In Figs. 5(a)–5(c), we plot the branching ratios for three of the four outgoing channels as a function of incoming k-vector. The fourth channel (reflection

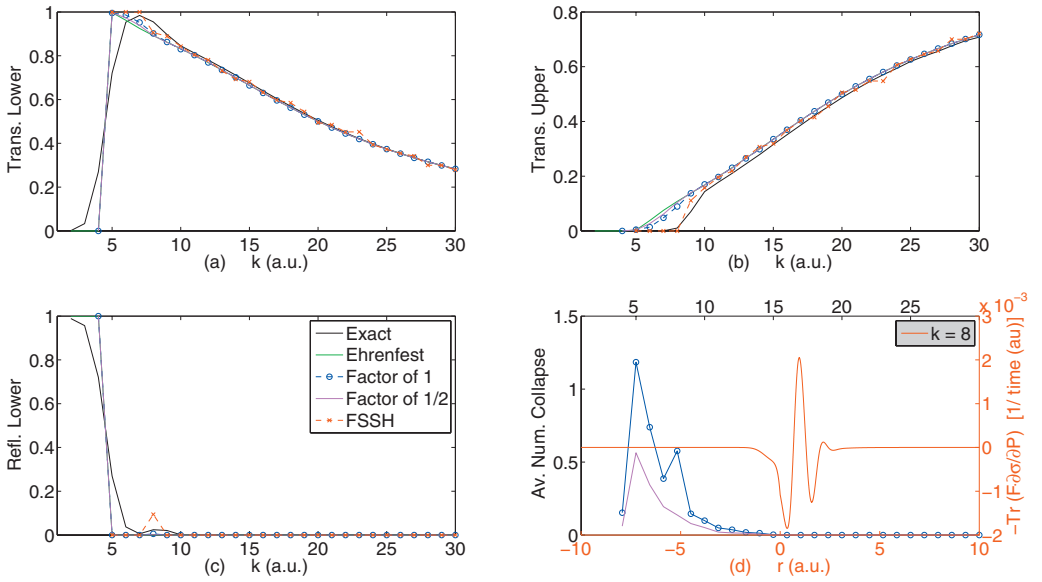

FIG. 5. Numerical results for the first Tully model problem with Hamiltonian in Eqs. (74)–(76), a simple avoided crossing. Exact results are shown in black, Ehrenfest in green, Tully's FSSH in red. Our results using our suggested decoherence rate Eqs. (52) and (72) ("factor of 1") are shown in blue and, for comparison, the results using a decoherence rate twice as small, Eqs. (70) and (72) ("factor or 1/2") are shown in magenta. In (a)–(c) we plot branching ratios. In (d), we plot the number of collapsing events as a function of the incoming k-value on the black axis: Eq. (52) is shown in blue and Eq. (70) is shown in magenta. On the red axis, as a function of real-space position, we plot the instantaneous value of $-\Sigma_{ij}F_{ij}(\partial\sigma_{ji}/\partial P) \equiv -\mathrm{Tr}(\mathbf{F}\cdot(\partial\boldsymbol{\sigma}/\partial P))$, which is proportional to the decoherence rate, for a standard Ehrenfest trajectory with an incoming k-value of 8.

on the upper surface) is not shown: the exact quantum results predict zero population in this channel, and our algorithm predicts a maximum population under 0.4%.

In the high energy regime, i.e., above $k>8.94$, all channels are open and, as noted by Tully,[5] FSSH and standard Ehrenfest both yield good branching ratios. Our algorithm also does well in this energy range. In Fig. 5(d), as a function of the incoming k-vector, we plot the average number of decoherence events undergone by one of our algorithm's trajectories. For $k=9$, the average is 0.15 for Eq. (72) and the average number of decoherence events decreases as k increases. Decreasing $1/\tau_d$ by a factor of 1/2 does not have any meaningful effect. Thus, our algorithm finds the correct branching ratios for $k>8.94$ because (i) it correctly recognizes that decoherence is not necessary and (ii) Ehrenfest does well.

In the low energy regime, below $k<8.9$ a.u., two interesting quantum mechanical features are apparent (in addition to tunneling through the barrier, which we ignore). First, the upper channel is closed, which leads to a kink in the transmission curves. This kink is stronger and more accurate using FSSH rather than our algorithm. Second, there is a small peak in the branching ratio for reflection on the lower surface. According to the FSSH formalism, this peak is caused by a particle that gets trapped in the interaction region and then is scattered backward. Like FSSH, we find a small peak in reflection near $k=8$ a.u.; according to our exact results, FSSH overestimates the height of the peak while our results underestimate the height. Interestingly, according to Fig. 5(d), trajectories at $k=7$, 8, or 9 undergo 0.39, 0.58, or 0.15 collapsing events using our suggested decoherence rate [Eq. (52)]. Thus, the basic collapsing criterion, $\mathrm{Tr}(\mathbf{F}\cdot(\partial\boldsymbol{\sigma}/\partial P))$, does seem to recognize when Ehrenfest dynamics is failing. Note that this peak in the number of collapsing event is missing when we decrease the rate $1/\tau_d$ by a factor of 1/2.

Despite these positive features, our algorithm [using Eq. (72)] does predict a nonzero amount (as high as 8%) of transmission into the upper state below 8.9 a.u. when the channel is rigorously closed. Thus, our branching ratios are not exact near this energy threshold. On a positive note, decoherence using Eq. (72) does give a correction to Ehrenfest dynamics (which predicts up to 11% population in closed channels). Overall, results from this model problem are encouraging qualitatively, and partially quantitatively.

B. Dual avoided crossing

The second model problem proposed by Tully is more difficult, a dual avoided crossing. The diabatic curves are defined by

$$V_{11}(x) = 0, \tag{77}$$

$$V_{22}(x) = -Ae^{-Bx^2} + E, \tag{78}$$

$$V_{12}(x) = V_{21}(x) = Ce^{-Dx^2}. \tag{79}$$

Here, $A=0.1$, $B=0.28$, $C=0.015$, $D=0.06$, and $E=0.05$. The adiabatic states are plotted in Fig. 4(b). After starting on the lower surface, the particle needs an initial k-vector satisfying $k>14.14$ a.u. to finish on the upper state.

The dual avoided crossing potential presents a challenge to our model because a particle in the potential will undergo Stueckelberg oscillations, and these oscillations cannot be fully described by any mean-field model. Moreover, because these oscillations are coherences and we are examining a nonadiabatic algorithm with the flavor of decoherence, certainly we cannot expect to capture the exact branching ratios.

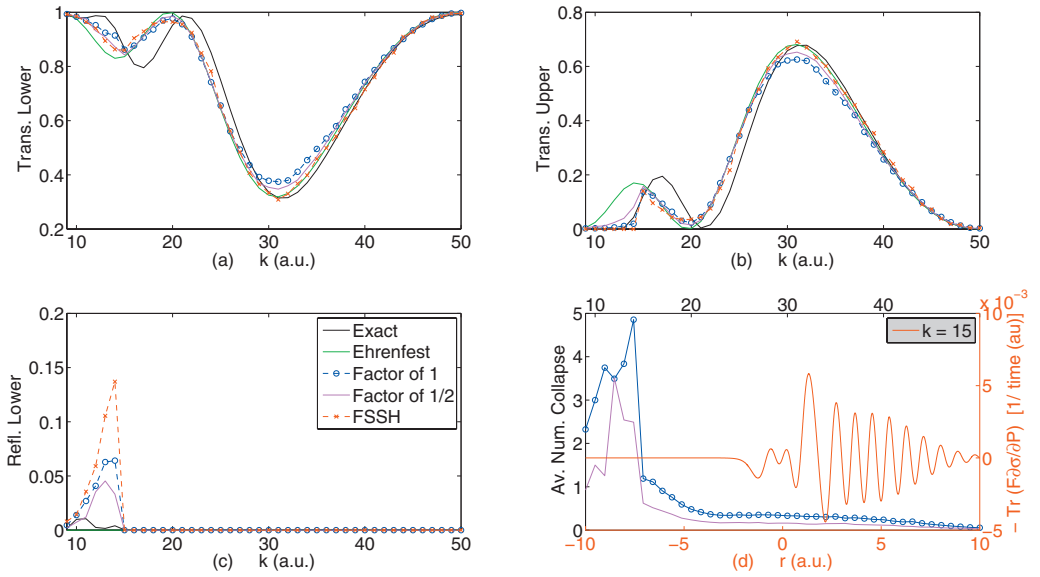

FIG. 6. The same as Fig. 5 only now for the Hamiltonian in Eqs. (77)–(79), a dual avoided crossing. In (d), the incoming k-value is now 15.

One key item to note about Fig. 6 is that Ehrenfest dynamics alone yields surprisingly accurate transmission and reflection probabilities at relatively high energies ($E>25$ a.u.). At such energies, presumably, decoherence is not very important and standard Ehrenfest dynamics is sufficient. Encouragingly, as for the first Tully problem, according to Fig. 6(d), our algorithm correctly predicts that the decoherence rate should be small for such large values of k_{inc}. This explains why our results match the exact results qualitatively. Quantitatively, our branching ratios are never wrong by more than 5% (over the whole range of k). We note that FSSH is correct to within 1% for the high energy range.

At low energies, the signature of quantum dynamics is a shift in the location of the first transmission peak (on the upper state) from $k=17$ a.u. (for the exact results) to $k=14$ a.u. (for the Ehrenfest results). In this energy regime, Ehrenfest fails badly because the upper channel should be closed at $k=14$ a.u. Hence, for this energy range, there is a need for a reliable dynamics algorithm that goes beyond mean field. Although we do not plot the data here, when we replace Eq. (52) with twice Eq. (46), our algorithm performs very poorly in this energy regime, much worse than Ehrenfest. Apparently, if we decohere at the absolute value rate $|\text{Tr}(\mathbf{F}\cdot(\partial\boldsymbol{\sigma}/\partial P))|$, we far overestimate any corrections to Ehrenfest dynamics and, as a consequence, the oscillations in the branching ratios are smeared away and our results become worse. This numerical result fits well with our frozen Gaussian interpretation of Ehrenfest dynamics: when $\text{Tr}(\mathbf{F}\cdot(\partial\boldsymbol{\sigma}/\partial P))$ is positive, the wave packets are, in fact, approaching each other and quantum coherences should not be discarded.

From Fig. 6, we observe that our algorithm using Eqs. (52) and (72) performs as well as FSSH in this low energy case. Both algorithms shift the transmission peak over to a higher k-vector (relative to pure Ehrenfest dynamics), but neither captures the exact overall shape of the true branching ratios, each with their own failures. On the one hand, just below $k<14$ a.u., our algorithm incorrectly predicts 2% transmission into the upper state, while FSSH always excludes closed channels. We also predict a small amount of population in the reflected upper channel ($<0.3\%$), which is forbidden as well (not shown). On the other hand, FSSH predicts 13% reflection into the lower state, while our algorithm predicts a branching ratio of about 6.4%. The correct value is $<1\%$. Finally, it is clear that reducing $1/\tau_d$ has a marginal effect on our final branching ratios, slightly worsening the transmission into the lower state at low energies but ameliorating the reflection onto the lower state.

Overall, this is a difficult test case for our algorithm, where all quantum coherences must be captured by Ehrenfest dynamics alone, and our correction can only address decoherences. Nevertheless, we find it encouraging that our results using Eqs. (52) and (72) resemble the exact results qualitatively, and each of our branching ratios in Fig. 6 is correct to within 5%.

C. Extended coupling with reflection

The third and final model problem suggested by Tully is one with extended coupling. This problem exemplifies the full strength of our algorithm because decoherence is absolutely crucial.[5,13,14]

The model diabatic potentials here are

$$V_{11}(x)=A, \tag{80}$$

$$V_{22}(x)=-A, \tag{81}$$

$$V_{12}(x)=V_{21}(x)=\begin{cases} Be^{Cx}, & x<0 \\ B(2-e^{-Cx}), & x>0, \end{cases} \tag{82}$$

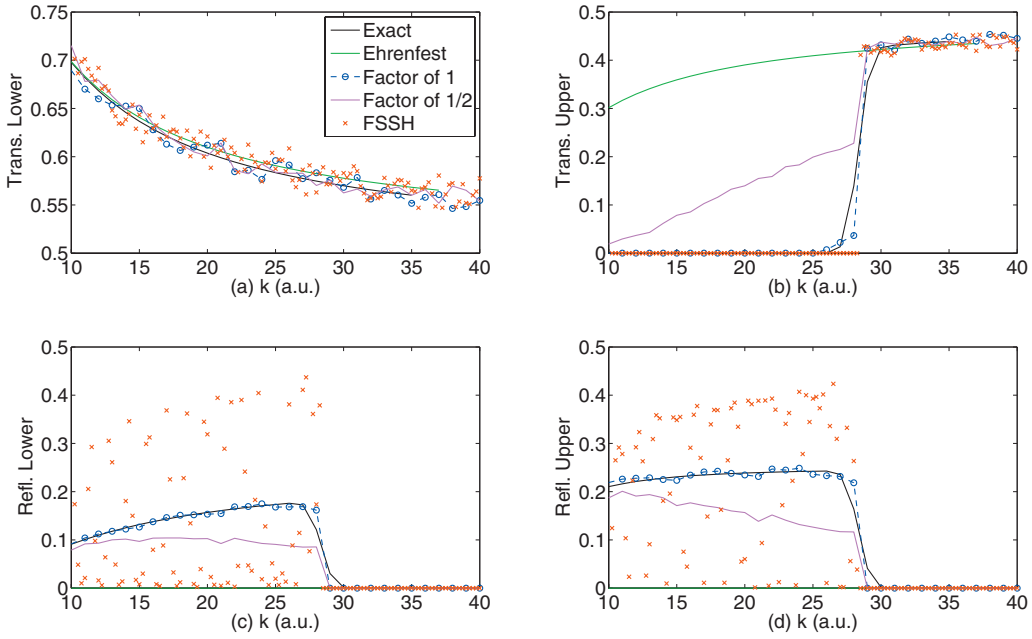

FIG. 7. (a)–(c) are the same as Fig. 5 only now for the Hamiltonian in Eqs. (80)–(82), a model problem with extended coupling. In (d), we plot the fourth channel, reflection on the upper surface.

where $A=6\times10^{-4}$, $B=0.1$, and $C=0.9$. The adiabatic curves are shown in Fig. 4(c).

The dynamics of a particle in this extended coupling potential is as follows. By energy conservation, after starting on the lower surface, a particle needs an initial k-vector satisfying $k>28.2$ a.u. to be transmitted on the upper surface. Immediately after the particle enters from the left, it feels the derivative coupling and begins to take on electronic density on the upper surface. As the particle approaches the origin, the derivative coupling vanishes, the two adiabatic states split in energy, and the particle must decide whether to transmit or reflect, depending on the electronic state of the system.

For the case that $k>28$, the particle is completely transmitted and, according to Fig. 7, all of the algorithms agree on the correct branching ratios. As was true for the previous problems, even basic Ehrenfest dynamics is accurate in this energy range because, given enough initial velocity, there is little decoherence. Regardless of the electronic state of the system, because the velocity of the particle is always positive at high energies, the nuclear wave packet remain nearly connected and can separate only slowly. Moreover, because the derivative coupling has vanished by the time the particle crosses the origin, the final branching ratios are already predetermined before the potential energy surfaces diverge.

By contrast, the situation when $k<28$ is very different. In this case, one can find wildly different results depending on the dynamics algorithm. First, standard Ehrenfest dynamics yields completely incorrect results, predicting only transmission and never reflection. Second, while FSSH predicts the correct transmission/reflection ratio, one finds strong oscillations in the reflection amplitudes between the different channels. Third, the Schwartz algorithm roughly infers the correct branching ratios (not shown), but with the proviso that one must impose a final collapse at infinity and close the upper channel artificially.

In contrast to other approaches, our algorithm using Eqs. (52) and (72) captures the branching ratio nearly exactly here and this example is the clearest demonstration possible of the strengths of our decoherence algorithm based on Ehrenfest dynamics. In order to understand why our algorithm gives good branching ratios, consider Fig. 8(a). Here, we see that, for $k\leq25$, the average trajectory undergoes one full collapsing event, but this number decreases as k increases. Thus, our algorithm has seemingly taken into account the necessary energy to climb up into the upper electronic state and has correctly identified the threshold energy, below which decoherence must occur as one wave packet is transmitted and another reflected.

The natural decoherence imparted by our algorithm is most easily quantified by measuring the decoherence rates for standard Ehrenfest trajectories. Thus, in Fig. 8(b), we plot $\int dt/\tau_d(t)$ [using Eq. (52)] along unmolested Ehrenfest trajectories. We do this for a series of increasing energy differences [B in Eq. (82)]. While the integral $\int dt/\tau_d(t)$ is a measure of the total probability of decohering away from the mean field, we mark with an x the threshold k-vector (k_{thresh}), which is necessary for the particle to be transmitted on the upper state.

From the data in Fig. 8(b), we see that when $B>0.2$, the total probability for decoherence is bigger than 1 for $k<k_{\text{thresh}}$. For smaller displacements, $B<0.2$, the algorithm is not perfect, but the probability for a decoherent collapse is still close to 1 for $k<k_{\text{thresh}}$ and the mixing of states is also small. We must, therefore, conclude that $-\text{Tr}(\mathbf{F}\cdot(\partial\boldsymbol{\sigma}/\partial P))$ provides a good measure of when to decohere, especially so

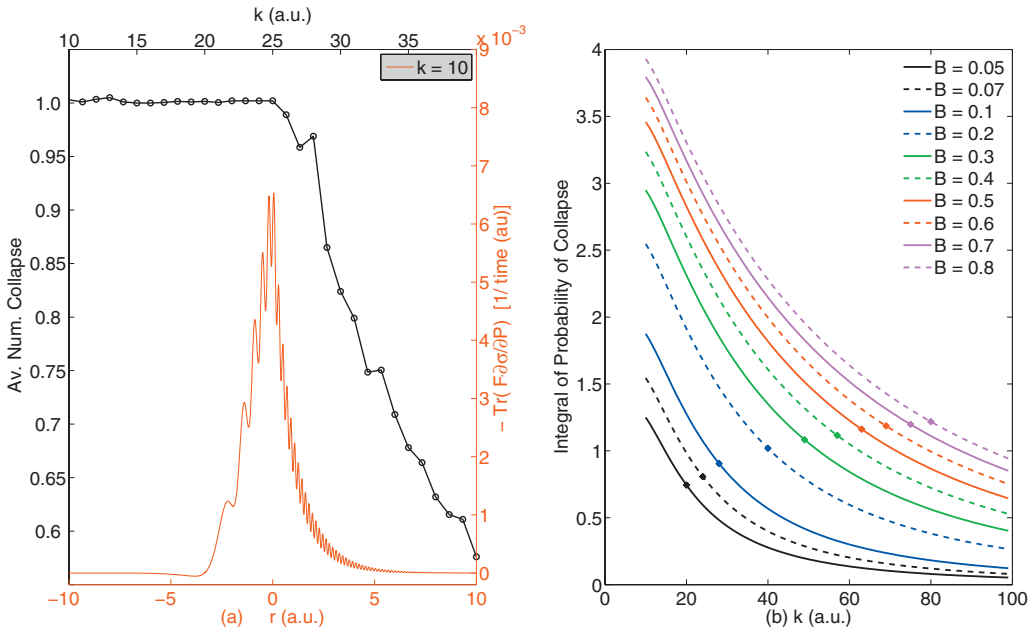

FIG. 8. (a) On the black axis, we plot the average number of collapsing events as a function of the incoming k-vector for the third Tully model problem [using Eqs. (52) and (72)]. On the red axis, we plot the instantaneous value of $-\mathrm{Tr}(\mathbf{F}\cdot(\partial\boldsymbol{\sigma}/\partial P))$ as a function of the nuclear position along a standard Ehrenfest trajectory with incoming $k=10$. (b) The integral—$\int dt(\mathrm{Tr}(\mathbf{F}\cdot(\partial\boldsymbol{\sigma}/\partial P)))\ \theta(-\mathrm{Tr}(\mathbf{F}\cdot(\partial\boldsymbol{\sigma}/\partial P)))$ along a standard, unmolested Ehrenfest trajectory for an array of different B values [B defined in Eq. (82)]. Here, θ is the Heaviside function. The points marked x denote the threshold k-vectors necessary for the incoming particle to be transmitted into the upper state for a given B value.

when the energy differences between electronic states grows large. This is a very encouraging development.

Finally, observe that when the rate of decoherence is decreased by a factor of 1/2, we can find very different and incorrect branching ratios. This further justifies the extra factor of 2 discussed in Sec. IV B 3.

Before concluding, we note that this model problem is the optimal example justifying why our algorithm cannot ignore forbidden hops and why we have implemented the nonlocal forbidden hop scheme as described in Sec. IV C. For this model problem, if one runs standard Ehrenfest dynamics until the classical turning point R_c of the upper adiabatic state [where $V_{22}(R_c)=E$], and then, at that unique point, one enforces a decoherence event so that the single trajectory collapses onto one of the two surfaces, one actually arrives at the correct branching ratios (not shown). Now, according to our algorithm, all collapsing events are stochastic, and if our algorithm requests a decoherence event at some position in space, there is no guarantee that this is the optimal position (which happens to exist only in this one-dimensional case). It would then be very arbitrary for us to either count or ignore all probability density in the upper state depending on whether we decohere just before or behind R_c.

VII. DISCUSSION AND SUMMARY

The principal results of this paper are (i) a computational means to check the accuracy of Ehrenfest dynamics on the fly and (ii) a new nonadiabatic dynamics algorithm that goes beyond mean-field and performs well on the Tully model problems. At bottom, we suggest running mean-field dynamics subject to stochastic decoherence events at the rate specified by Eqs. (52) and (72). While this approach is very similar in spirit to the approach in Refs. 13 and 14, we emphasize that, in contrast to the Schwartz algorithm, our method has no adjustable parameters. Instead, in order to calculate the decoherence rate, our algorithm propagates more variables than the standard Ehrenfest routine. In particular, we propagate the mixed nuclear-electronic derivatives ($\partial\boldsymbol{\sigma}/\partial R$ and $\partial\boldsymbol{\sigma}/\partial P$) that hold crucial information about nuclear-electronic correlation.

The decoherence rate underlying our algorithm [Eq. (52)] has been derived in two different ways: (i) by comparing the equation of motion in mixed nuclear-electronic phase space for Ehrenfest dynamics versus partial Wigner transform dynamics[20,21] and (ii) by interpreting Ehrenfest dynamics as corresponding to a set of frozen Gaussian wave packets that are allowed to separate. Because the same expression can be found in multiple ways, and because the numerical results for a few model problems are successful, we believe that our nonadiabatic algorithm has a good chance to succeed for many chemical applications.

In the future, the most important next step forward will be benchmarking this nonadiabatic algorithm over a set of many different potential energy surfaces where exact quantum results can be made and compared. In particular, it will be crucial to test this algorithm on surfaces with more than one nuclear degree of freedom. Besides branching ratios, we must also check for detailed balance and the relative populations of electronic states in the presence of a boson bath. Detailed balance holds approximately for the FSSH algorithm.[41]

Although we have hope that our algorithm will prove a step forward in our understanding of mixed nonadiabatic dynamics, there is some cause for concern. First, the examples

in this paper clearly demonstrate that this algorithm does not entirely prevent small populations arising in closed channels. Second, because decoherence throws away correlations between adiabatic states, there will be necessary limits to what this algorithm can achieve. For these reasons, we are currently designing a separate algorithm that incorporates the decoherence rate in Eq. (52) within the FSSH formalism so as to better connect with the standard surface-hopping formalism and deepen our understanding of semiclassical nonadiabatic dynamics.[42]

If, however, the algorithm presented here does perform well over a broad range of dynamics calculations, then five conceptual issues should be addressed in the future in order to improve this method. First, regarding computational cost, as written above, our algorithm requires second derivatives of the potential energy surface [i.e., Eqs. (40) and (41)]. This need for second derivatives will make on the fly electronic-structure calculations much more expensive. Future work should investigate whether the second-derivative terms can be approximated so as to make the dynamics algorithm more computationally efficient. Although usually one cannot achieve "something for nothing," one would strongly prefer a decoherence algorithm which required only first derivatives of the potential energy surface.

Second, in this paper, we have focused only on the case of two electronic states. In the future, this algorithm should be extended to the case of three or more electronic states. Looking back at the algorithm above, we find that there is no obvious and unique prescription for such an extension. Instead, there are many possibilities for how one could treat the case of three or more wave packets decohering on multiple surfaces. For this reason, we have hesitated to hypothesize an algorithm without having exact quantum dynamics calculations to compare against.

Third, regarding the question of representation, in this paper, all of our works have assumed an adiabatic representation, and Tully and co-workers have long argued that FSSH works best in an adiabatic (rather than diabatic) representation.[6] It will be very interesting, and perhaps fruitful, to explore whether the algorithm and ideas presented here can be transported in a meaningful way to a diabatic representation. One might hope that such an approach would be possible because Ehrenfest dynamics works equally well in both representations.

Fourth, as presented in this paper, our dynamics algorithm is not time reversible. In order for the algorithm to be time reversible, we need a means to combine two separate, independent trajectories into a single coherent trajectory. If such a feat were possible, this algorithm might also be able to quantitatively model difficult coherences, including Stueckelberg oscillations. Although it may be impossible, future work should at least attempt to see if and how two separated trajectories may subsequently be recombined.

Fifth and finally, from a purely theoretical perspective, it would be very satisfying if one could demonstrate a deeper connection between our trajectories and Kapral's "momentum jump" trajectories[20,21] for propagating the partial Wigner transform. Moreover, if such a connection were possible, we might also find a correction to this algorithm.

In summary, this paper has presented (i) a new formalism for quantifying the error of Ehrenfest dynamics and (ii) a new approach for mixed quantum-classical dynamics wherein there is a natural rate for stochastic decoherence events—without any adjustable parameters—along mean-field trajectories. Our preliminary numerical results are encouraging. Because so many problems in chemistry involve electron transfer or electronic relaxation, where nonadiabatic dynamics can be crucial, there is a strong motivation to refine and benchmark this algorithm in the future. Although Eqs. (40), (41), and (52) are currently in their infancy, our hope is that this paper presents significantly new ideas to help push forward mixed nuclear-electronic dynamics.

ACKNOWLEDGMENTS

I thank Ben Schwartz, Neil Shenvi, Ryan Steele, John Tully, Bill Miller, Todd Martinez, David Chandler, Ignacio Franco, David Tannor, Mark Ratner, and Abraham Nitzan for very illuminating discussions and feedback. In particular, I thank Neil Shenvi for pointing out the similarities between Eqs. (46) and (52), and I thank Ben Schwartz for suggesting this problem to me. This research was supported by Professor Mark Ratner and grants from the chemistry divisions of NSF and ONR. I dedicate this article to my parents, Rose and Danny Subotnik.

APPENDIX A: CALCULATION OF EXACT QUANTUM RESULTS

The exact quantum results in this paper have been computed in MATLAB using a finite one-dimensional grid and a fast Fourier transformation to represent the momentum operator. No matter the value of k ($k \geq 4$), we have chosen the width of the incoming wave packet to be 1 a.u. and we have checked that the resulting branching ratios are nearly unchanged if we change the width to 2 a.u. After diagonalizing the total Hamiltonian and propagating the wave packet for a small time Δt, we used a masking function along the boundaries of the grid to eliminate outgoing particle density, while simultaneously measuring the distribution of this flux over the different electronic states. Overall, we estimate that our branching ratios are correct to within 1%. More accurate results are certainly possible (see, e.g., Ref. 43).

APPENDIX B: CALCULATION OF $\partial\sigma/\partial R$ AND $\partial\sigma/\partial P$

In this section, we will not limit ourselves to a single classical nucleus and, instead, we will compute the equation of motion for the mixed nuclear-electronic derivatives subject to the general case of many nuclear degrees of freedom. Overhead arrows will denote nuclear vectors, bold face denotes electronic matrices, superscript Greek indices are nuclear, and subscript Roman indices are electronic. For convenience, we set $\hbar = 1$.

1. Equation of motion for $\partial\sigma/\partial P$

Suppose that at time t_0, a mixed quantum-classical Ehrenfest trajectory starts out with coordinates $\vec{R}_0, \vec{P}_0, \boldsymbol{\sigma}_0$

and evolves to coordinates $\vec{R}_1, \vec{P}_1, \sigma_1$ at time $t_1 = t_0 + dt$. According to the Ehrenfest equations of motion, to first order in dt, we have

$$U(t_1,t_0):\begin{pmatrix}\vec{R}_0\\ \vec{P}_0\end{pmatrix} \mapsto \begin{pmatrix}\vec{R}_1\\ \vec{P}_1\end{pmatrix}$$

$$\begin{pmatrix}\vec{R}_1\\ \vec{P}_1\end{pmatrix} = \begin{pmatrix}\vec{R}_0 + \dfrac{\vec{P}_0}{M}dt\\ \vec{P}_0 - \displaystyle\sum_{kl} \sigma_{kl}(\vec{R}_0,\vec{P}_0,t_0)\vec{F}_{lk}(\vec{R}_0)dt\end{pmatrix}, \tag{B1}$$

where $U(t_1,t_0)$ denotes the time evolution operator.

Let $\{\vec{e}_R^{\beta}, \vec{e}_P^{\beta}\}$ be a basis for classical phase space. In order to calculate $\partial\sigma_{ij}/\partial P$, we must consider how a small change in the initial nuclear momentum affects the final electronic state (see Fig. 9).

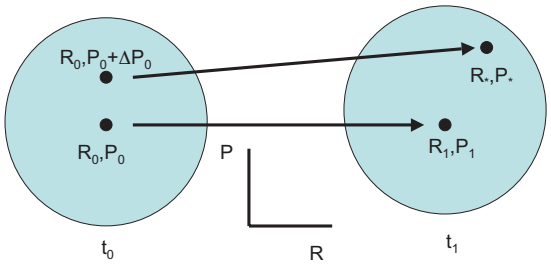

FIG. 9. A graphical representation of the time evolution around a single trajectory.

In practice, we will find that $\partial\sigma_{ij}/\partial P$ may be computed through a series of Taylor series expansions. We start by perturbing $\vec{P}_0$ by $\Delta\vec{P}_0 = \Sigma_\beta \delta P^\beta \vec{e}_P^{\beta}$. The resulting change in the trajectory of the nuclear position and momentum is

$$U(t_1,t_0):\begin{pmatrix}\vec{R}_0\\ \vec{P}_0 + \Delta\vec{P}_0\end{pmatrix} \mapsto \begin{pmatrix}\vec{R}_*\\ \vec{P}_*\end{pmatrix} = \begin{pmatrix}\vec{R}_0 + \dfrac{(\vec{P}_0 + \Delta\vec{P}_0)}{M}dt\\ \vec{P}_0 + \Delta\vec{P}_0 - \displaystyle\sum_{kl} \sigma_{kl}(\vec{R}_0,\vec{P}_0 + \Delta\vec{P}_0,t_0)\vec{F}_{lk}(\vec{R}_0)dt\end{pmatrix}$$

$$= \begin{pmatrix}\vec{R}_1 + \dfrac{\Delta\vec{P}_0}{M}dt\\ \vec{P}_1 + \Delta\vec{P}_0 - \displaystyle\sum_{\beta kl} \left.\frac{\partial\sigma_{kl}}{\partial P^\beta}\right|_{t_0} \vec{F}_{lk}(\vec{R}_0)\,\delta P^\beta dt\end{pmatrix}. \tag{B2}$$

For the perturbed nuclear trajectory in Eq. (B2), we seek the change in the electronic density. To first order, using the equation of motion for $\boldsymbol{\sigma}$ [Eq. (9)], we have

$$\sigma_{rs}(\vec{R}_*,\vec{P}_*,t_1) = \sigma_{rs}(\vec{R}_0,\vec{P}_0 + \Delta\vec{P}_0,t_0) + \dot{\sigma}_{rs}(\vec{R}_0,\vec{P}_0 + \Delta\vec{P}_0,t_0)dt. \tag{B3}$$

We now perform several Taylor expansions. The right hand side of Eq. (B3) becomes

$$\begin{aligned}\mathrm{RHS} = {}& \sigma_{rs}|_{t_0} + \sum_\beta \left.\frac{\partial\sigma_{rs}}{\partial P^\beta}\right|_{t_0} \delta P^\beta \\ & - i[\mathbf{H}(\vec{R}_0), \boldsymbol{\sigma}(\vec{R}_0,\vec{P}_0 + \Delta\vec{P}_0,t_0)]_{rs}dt \\ & - \sum_\alpha \frac{(P_0^\alpha + \delta P^\alpha)}{M}[\mathbf{d}^\alpha(\vec{R}_0), \boldsymbol{\sigma}(\vec{R}_0,\vec{P}_0 + \Delta\vec{P}_0,t_0)]_{rs}dt\end{aligned} \tag{B4}$$

while the left-hand side of Eq. (B3) is expanded as

$$\begin{aligned}& = \sigma_{rs}|_{t_0} + \sum_\beta \left.\frac{\partial\sigma_{rs}}{\partial P^\beta}\right|_{t_0} \delta P^\beta - i[\mathbf{H}(\vec{R}_0), \boldsymbol{\sigma}|_{t_0}]_{rs}dt \\ & - \sum_\alpha \frac{P_0^\alpha}{M}[\mathbf{d}^\alpha(\vec{R}_0), \boldsymbol{\sigma}|_{t_0}]_{rs}dt \\ & - i\sum_\beta \left[\mathbf{H}(\vec{R}_0), \left.\frac{\partial\boldsymbol{\sigma}}{\partial P^\beta}\right|_{t_0}\right]_{rs} \delta P^\beta dt \\ & - \sum_{\alpha\beta} \frac{\vec{P}_0^\alpha}{M}\left[\mathbf{d}^\alpha(\vec{R}_0), \left.\frac{\partial\boldsymbol{\sigma}}{\partial P^\beta}\right|_{t_0}\right]_{rs} \delta P^\beta dt \\ & - \sum_\beta \frac{1}{M}[\mathbf{d}^\beta(\vec{R}_0), \boldsymbol{\sigma}|_{t_0}]_{rs}\delta P^\beta dt,\end{aligned} \tag{B5}$$

$$\mathrm{LHS} = \sigma_{rs}\left(\vec{R}_1 + \frac{\Delta\vec{P}_0 dt}{M}, \vec{P}_1 + \Delta\vec{P}_0 - \sum_{\beta kl}\left.\frac{\partial\sigma_{kl}}{\partial P^\beta}\right|_{t_0}\vec{F}_{lk}(\vec{R}_0)\delta P^\beta dt, t_1\right) \tag{B6}$$

$$= \sigma_{rs}|_{t_1} + \sum_\beta \left.\frac{\partial\sigma_{rs}}{\partial P^\beta}\right|_{t_1}\delta P^\beta + \sum_\beta \frac{dt}{M}\left.\frac{\partial\sigma_{rs}}{\partial R^\beta}\right|_{t_1}\delta P^\beta - \sum_{\beta\alpha kl}\left.\frac{\partial\sigma_{rs}}{\partial P^\alpha}\right|_{t_1}\left.\frac{\partial\sigma_{kl}}{\partial P^\beta}\right|_{t_0}F^\alpha_{lk}(\vec{R}_0)dt\,\delta P^\beta. \tag{B7}$$

Putting together Eqs. (B5) and (B7) and using (to first order)

$$\sigma_{rs}|_{t_1} = \sigma_{rs}|_{t_0} - i[\mathbf{H}(\vec{R}_0), \boldsymbol{\sigma}|_{t_0}]_{rs}dt - \sum_\alpha \frac{P_0^\alpha}{M}[\mathbf{d}^\alpha(\vec{R}_0), \boldsymbol{\sigma}|_{t_0}]_{rs}dt, \tag{B8}$$

we conclude that the equation of motion for $\partial\sigma_{ij}/\partial P$ is

$$\begin{aligned}\frac{d}{dt}\frac{\partial\sigma_{rs}}{\partial P^\beta} &\equiv \frac{1}{dt}\left(\left.\frac{\partial\sigma_{rs}}{\partial P^\beta}\right|_{t_1} - \left.\frac{\partial\sigma_{rs}}{\partial P^\beta}\right|_{t_0}\right)\\ &= -i\left[\mathbf{H}(\vec{R}_0), \left.\frac{\partial\boldsymbol{\sigma}}{\partial P^\beta}\right|_{t_0}\right]_{rs} - \sum_\alpha \frac{P_0^\alpha}{M}\left[\mathbf{d}^\alpha(\vec{R}_0), \left.\frac{\partial\boldsymbol{\sigma}}{\partial P^\beta}\right|_{t_0}\right]_{rs} - \frac{1}{M}[\mathbf{d}^\beta(\vec{R}_0), \boldsymbol{\sigma}|_{t_0}]_{rs} - \frac{1}{M}\left.\frac{\partial\sigma_{rs}}{\partial R^\beta}\right|_{t_1}\\ &\quad + \sum_{\alpha kl}\left.\frac{\partial\sigma_{rs}}{\partial P^\alpha}\right|_{t_1}\left.\frac{\partial\sigma_{kl}}{\partial P^\beta}\right|_{t_0}F^\alpha_{lk}(\vec{R}_0).\end{aligned} \tag{B9}$$

Setting $t_0 = t_1$, we arrive at the final equation of motion [Eq. (41)]. Note that in the process of deriving Eq. (B9), we have found that $\partial\sigma_{ij}/\partial P$ is fundamentally correlated with $\partial\sigma_{ij}/\partial R$.

2. Equation of motion for $\partial\sigma/\partial R$

Repeating the above analysis, only substituting spatial derivatives for momentum derivatives, we consider the effect in phase space of a small initial change in the spatial coordinate, $\Delta\vec{R}_0 = \Sigma_\beta \delta R^\beta \vec{e}^\beta_R$,

$$\begin{aligned}U(t_1,t_0):\begin{pmatrix}\vec{R}_0 + \Delta\vec{R}_0\\ \vec{P}_0\end{pmatrix} \to \begin{pmatrix}\vec{R}_*\\ \vec{P}_*\end{pmatrix} &= \begin{pmatrix}\vec{R}_0 + \Delta\vec{R}_0 + \dfrac{\vec{P}_0}{M}dt\\ \vec{P}_0 - \sum_{kl}\sigma_{kl}(\vec{R}_0 + \Delta\vec{R}_0, \vec{P}_0, t_0)\vec{F}_{lk}(\vec{R}_0 + \Delta\vec{R}_0, \vec{P}_0, t_0)dt\end{pmatrix}\\ &= \begin{pmatrix}\vec{R}_1 + \Delta\vec{R}_0\\ \vec{P}_1 - \sum_{\beta kl}\left.\dfrac{\partial\sigma_{kl}}{\partial R^\beta}\right|_{t_0}\vec{F}_{lk}(\vec{R}_0)dt\,\delta R^\beta - \sum_{\beta kl}\sigma_{kl}|_{t_0}\left.\dfrac{\partial\vec{F}_{lk}}{\partial R^\beta}\right|_{\vec{R}_0}dt\,\delta R^\beta\end{pmatrix}.\end{aligned} \tag{B10}$$

We also consider the corresponding change in the electronic density matrix

$$\sigma_{rs}(\vec{R}_*, \vec{P}_*, t_1) = \sigma_{rs}(\vec{R}_0 + \Delta\vec{R}_0, \vec{P}_0, t_0) + \dot{\sigma}_{rs}(\vec{R}_0 + \Delta\vec{R}_0, \vec{P}_0, t_0)dt. \tag{B11}$$

Expanding, the right hand side of Eq. (B11) becomes

$$\begin{aligned}\mathrm{RHS} &= \sigma_{rs}|_{t_0} + \sum_\beta \left.\frac{\partial\sigma_{rs}}{\partial R^\beta}\right|_{t_0}\delta R^\beta - i[\mathbf{H}(\vec{R}_0 + \Delta\vec{R}_0), \boldsymbol{\sigma}(\vec{R}_0 + \Delta\vec{R}_0, \vec{P}_0, t_0)]_{rs}dt - \sum_\alpha \frac{P_0^\alpha}{M}[\mathbf{d}^\alpha(\vec{R}_0 + \Delta\vec{R}_0), \boldsymbol{\sigma}(\vec{R}_0 + \Delta\vec{R}_0, \vec{P}_0, t_0)]_{rs}dt\\ &= \sigma_{rs}|_{t_0} + \sum_\beta \left.\frac{\partial\sigma_{rs}}{\partial R^\beta}\right|_{t_0}\delta R^\beta - i[\mathbf{H}(\vec{R}_0), \boldsymbol{\sigma}|_{t_0}]_{rs}dt - \sum_\alpha \frac{P_0^\alpha}{M}[\mathbf{d}^\alpha(\vec{R}_0), \boldsymbol{\sigma}|_{t_0}]_{rs}dt - i\sum_\beta\left[\mathbf{H}(\vec{R}_0), \left.\frac{\partial\boldsymbol{\sigma}}{\partial R^\beta}\right|_{t_0}\right]_{rs}\delta R^\beta dt\\ &\quad - i\sum_\beta[\mathbf{F}^\beta(\vec{R}_0), \boldsymbol{\sigma}|_{t_0}]_{rs}\delta R^\beta dt - \sum_{\beta\alpha}\frac{\vec{P}_0^\alpha}{M}\left[\mathbf{d}^\alpha(\vec{R}_0), \left.\frac{\partial\boldsymbol{\sigma}}{\partial R^\beta}\right|_{t_0}\right]_{rs}\delta R^\beta dt - \sum_{\beta\alpha}\frac{\vec{P}_0^\alpha}{M}\left[\frac{\partial\mathbf{d}^\alpha(\vec{R}_0)}{\partial R^\beta}, \boldsymbol{\sigma}|_{t_0}\right]_{rs}\delta R^\beta dt,\end{aligned} \tag{B12}$$

and the left-hand side of Eq. (B11) becomes

$$\text{LHS} = \sigma_{rs}\left(\vec{R}_1 + \Delta\vec{R}_0, \vec{P}_1 - \sum_{\beta kl} \left.\frac{\partial \sigma_{kl}}{\partial R^\beta}\right|_{t_0} \vec{F}_{lk}(\vec{R}_0)dt\,\delta R^\beta - \sum_{\beta kl} \sigma_{kl}|_{t_0} \frac{\partial \vec{F}_{lk}}{\partial R^\beta}(\vec{R}_0)dt\,\delta R^\beta, t_1\right)$$

$$= \sigma_{rs}|_{t_1} + \sum_\beta \left.\frac{\partial \sigma_{rs}}{\partial R^\beta}\right|_{t_1} \delta R^\beta - \sum_{\beta\alpha kl} \left.\frac{\partial \sigma_{rs}}{\partial P^\alpha}\right|_{t_1} \left.\frac{\partial \sigma_{kl}}{\partial R^\beta}\right|_{t_0} F^\alpha_{lk}(\vec{R}_0)dt\,\delta R^\beta - \sum_{\beta\alpha kl} \left.\frac{\partial \sigma_{rs}}{\partial P^\alpha}\right|_{t_1} \sigma_{kl}|_{t_0} \left.\frac{\partial F^\alpha_{lk}}{\partial R^\beta}\right| (\vec{R}_0)dt\,\delta R^\beta. \tag{B13}$$

Combining Eqs. (B12) and (B13) and using Eq. (B8), we find the equation of motion for the change in $\boldsymbol{\sigma}$ with respect to spatial derivatives

$$\frac{d}{dt}\frac{\partial \sigma_{rs}}{\partial R^\beta} \equiv \frac{1}{dt}\left(\left.\frac{\partial \sigma_{rs}}{\partial R^\beta}\right|_{t_1} - \left.\frac{\partial \sigma_{rs}}{\partial R^\beta}\right|_{t_0}\right) = -i\left[\mathbf{H}(\vec{R}_0), \left.\frac{\partial \boldsymbol{\sigma}}{\partial R^\beta}\right|_{t_0}\right]_{rs} - i[\mathbf{F}^\beta(\vec{R}_0), \boldsymbol{\sigma}|_{t_0}]_{rs} - \sum_\alpha \frac{\vec{P}^\alpha_0}{M}\left[\mathbf{d}^\alpha(\vec{R}_0), \left.\frac{\partial \boldsymbol{\sigma}}{\partial R^\beta}\right|_{t_0}\right]_{rs}$$

$$- \sum_\alpha \frac{\vec{P}^\alpha_0}{M}\left[\frac{\partial \mathbf{d}^\alpha(\vec{R}_0)}{\partial R^\beta}, \boldsymbol{\sigma}|_{t_0}\right]_{rs} + \sum_{\alpha kl} \left.\frac{\partial \sigma_{rs}}{\partial P^\alpha}\right|_{t_1} \left.\frac{\partial \sigma_{kl}}{\partial R^\beta}\right|_{t_0} F^\alpha_{lk}(\vec{R}_0) + \sum_{\alpha kl} \left.\frac{\partial \sigma_{rs}}{\partial P^\alpha}\right|_{t_1} \sigma_{kl}|_{t_0} \frac{\partial F^\alpha_{lk}}{\partial R^\beta}(\vec{R}_0). \tag{B14}$$

Finally, we set $t_0 = t_1$ and the result is Eq. (40).

[1] A. M. Wodtke, J. C. Tully, and D. J. Auerbach, Int. Rev. Phys. Chem. **23**, 513 (2004).
[2] A. D. McLachlan, Mol. Phys. **8**, 39 (1964).
[3] H. D. Meyer and W. H. Miller, J. Chem. Phys. **72**, 2272 (1980).
[4] J. C. Tully and R. K. Preston, J. Chem. Phys. **55**, 562 (1971).
[5] J. C. Tully, J. Chem. Phys. **93**, 1061 (1990).
[6] J. C. Tully, Faraday Discuss. **110**, 407 (1998).
[7] F. Webster, P. J. Rossy, and R. A. Friesner, Comput. Phys. Commun. **63**, 494 (1991).
[8] F. Webster, E. T. Wang, P. J. Rossy, and R. A. Friesner, J. Chem. Phys. **100**, 4835 (1994).
[9] O. V. Prezhdo and P. J. Rossky, J. Chem. Phys. **107**, 825 (1997).
[10] K. F. Wong and P. J. Rossky, J. Chem. Phys. **116**, 8418 (2002).
[11] K. F. Wong and P. J. Rossky, J. Chem. Phys. **116**, 8429 (2002).
[12] O. V. Prezhdo, J. Chem. Phys. **111**, 8366 (1999).
[13] M. J. Bedard-Hearn, R. E. Larsen, and B. J. Schwartz, J. Chem. Phys. **123**, 234106 (2005).
[14] R. E. Larsen, M. J. Bedard-Hearn, and B. J. Schwartz, J. Phys. Chem. B **110**, 20055 (2006).
[15] H. D. Meyer and W. H. Miller, J. Chem. Phys. **70**, 3214 (1979).
[16] G. Stock and M. Thoss, Phys. Rev. Lett. **78**, 578 (1997).
[17] W. H. Miller, J. Phys. Chem. A **113**, 1405 (2009).
[18] T. J. Martinez, M. Ben-Nun, and R. D. Levine, J. Phys. Chem. **100**, 7884 (1996).
[19] M. Ben-Nun and T. J. Martinez, J. Chem. Phys. **112**, 6113 (2000).
[20] R. Kapral and G. Ciccotti, J. Chem. Phys. **110**, 8919 (1999).
[21] S. Nielsen, R. Kapral, and G. Ciccotti, J. Chem. Phys. **112**, 6543 (2000).
[22] I. V. Z. Aleksandrov, Z. Naturforsch. A **36A**, 902 (1981).
[23] W. Boucher and J. Traschen, Phys. Rev. D **37**, 3522 (1988).
[24] W. Y. Zhang and R. Balescu, J. Plasma Phys. **40**, 199 (1988).
[25] R. Balescu and W. Y. Zhang, J. Plasma Phys. **40**, 215 (1988).
[26] A. Anderson, Phys. Rev. Lett. **74**, 621 (1995).
[27] O. V. Prezhdo and V. V. Kisil, Phys. Rev. A **56**, 162 (1997).
[28] C. C. Martens and J. Y. Fang, J. Chem. Phys. **106**, 4918 (1997).
[29] A. Donoso and C. C. Martens, J. Phys. Chem. **102**, 4291 (1998).
[30] D. A. Micha and B. Thorndyke, Int. J. Quantum Chem. **90**, 759 (2002).
[31] Y. L. Volobuev, M. D. Hack, M. S. Topaler, and D. G. Truhlar, J. Chem. Phys. **112**, 9716 (2000).
[32] M. D. Hack and D. G. Truhlar, J. Chem. Phys. **114**, 2894 (2001).
[33] A. W. Jasper, M. D. Hack, and D. G. Truhlar, J. Chem. Phys. **115**, 1804 (2001).
[34] C. Zhu, A. W. Jasper, and D. G. Truhlar, J. Chem. Phys. **120**, 5543 (2004).
[35] C. Zhu, S. Nangia, A. W. Jasper, and D. G. Truhlar, J. Chem. Phys. **121**, 7658 (2004).
[36] A. W. Jasper and D. G. Truhlar, J. Chem. Phys. **123**, 064103 (2005).
[37] I. Horenko, C. Salzmann, B. Schmidt, and C. Schutte, J. Chem. Phys. **117**, 11075 (2002).
[38] E. J. Heller, J. Chem. Phys. **75**, 2923 (1981).
[39] B. J. Schwartz, E. R. Bittner, O. V. Prezhdo, and P. J. Rossky, J. Chem. Phys. **104**, 5942 (1996).
[40] E. Neria and A. Nitzan, J. Chem. Phys. **99**, 1109 (1993).
[41] J. R. Schmidt, P. V. Parandekar, and J. C. Tully, J. Chem. Phys. **129**, 044104 (2008).
[42] J. E. Subotnik and N. Shenvi (unpublished).
[43] D. Kosloff and R. Kosloff, J. Comput. Phys. **52**, 35 (1983).